

# UCSF

## UC San Francisco Previously Published Works

### Title

Respiratory complex I regulates dendritic cell maturation in explant model of human tumor immune microenvironment.

### Permalink

<https://escholarship.org/uc/item/0sz2x90w>

### Journal

Journal for ImmunoTherapy of Cancer, 12(4)

### Authors

Turpin, Rita

Liu, Ruixian

Munne, Pauliina

et al.

### Publication Date

2024-04-11

### DOI



10.1136/jitc-2023-008053

### Copyright Information

This work is made available under the terms of a Creative Commons Attribution-NonCommercial License, available at <https://creativecommons.org/licenses/by-nc/4.0/>

Peer reviewed

# Respiratory complex I regulates dendritic cell maturation in explant model of human tumor immune microenvironment

Rita Turpin,<sup>1</sup> Ruixian Liu,<sup>1</sup> Pauliina M Munne,<sup>1</sup> Aino Peura,<sup>1</sup> Jenna H Rannikko,<sup>2</sup> Gino Philips,<sup>3</sup> Bram Boeckx,<sup>4</sup> Natasha Salmelin,<sup>1</sup> Elina Hurskainen,<sup>1</sup> Iida Suleymanova,<sup>1</sup> July Aung,<sup>5</sup> Elisa M Vuorinen,<sup>6</sup> Laura Lehtinen,<sup>6</sup> Minna Mutka,<sup>7</sup> Panu E Kovanen,<sup>8</sup> Laura Niinikoski,<sup>9</sup> Tuomo J Meretoja,<sup>9</sup> Johanna Mattson,<sup>10</sup> Satu Mustjoki <sup>11,12</sup> Päivi Saavalainen,<sup>6</sup> Andrei Goga,<sup>13</sup> Diether Lambrechts,<sup>14</sup> Jeroen Pouwels,<sup>1</sup> Maija Hollmén,<sup>2</sup> Juha Klefström <sup>1,15</sup>

**To cite:** Turpin R, Liu R, Munne PM, *et al.* Respiratory complex I regulates dendritic cell maturation in explant model of human tumor immune microenvironment. *Journal for ImmunoTherapy of Cancer* 2024;**12**:e008053. doi:10.1136/jitc-2023-008053

► Additional supplemental material is published online only. To view, please visit the journal online (<https://doi.org/10.1136/jitc-2023-008053>).

RL and PMM contributed equally.

Accepted 04 March 2024



© Author(s) (or their employer(s)) 2024. Re-use permitted under CC BY-NC. No commercial re-use. See rights and permissions. Published by BMJ.

For numbered affiliations see end of article.

## Correspondence to

Dr Juha Klefström;  
juha.klefstrom@helsinki.fi

## ABSTRACT

**Background** Combining cytotoxic chemotherapy or novel anticancer drugs with T-cell modulators holds great promise in treating advanced cancers. However, the response varies depending on the tumor immune microenvironment (TIME). Therefore, there is a clear need for pharmacologically tractable models of the TIME to dissect its influence on mono- and combination treatment response at the individual level.

**Methods** Here we establish a patient-derived explant culture (PDEC) model of breast cancer, which retains the immune contexture of the primary tumor, recapitulating cytokine profiles and CD8+T cell cytotoxic activity.

**Results** We explored the immunomodulatory action of a synthetic lethal BCL2 inhibitor venetoclax+metformin drug combination *ex vivo*, discovering metformin cannot overcome the lymphocyte-depleting action of venetoclax. Instead, metformin promotes dendritic cell maturation through inhibition of mitochondrial complex I, increasing their capacity to co-stimulate CD4+T cells and thus facilitating antitumor immunity.

**Conclusions** Our results establish PDECs as a feasible model to identify immunomodulatory functions of anticancer drugs in the context of patient-specific TIME.

## INTRODUCTION

While a common denominator of cancer is a dysregulation of the tumor immune microenvironment (TIME), the actual composition and function of the TIME is both tumor type-specific and patient-specific.<sup>1</sup> Characterizing the TIME is improving the stratification of patients who may respond to immunomodulatory monotherapies, like anti-CTLA-4 or anti-programmed cell death 1 (PD-1)/programmed death ligand 1 (PD-L1).<sup>2</sup> However, it is increasingly clear that the TIME also has a strong role in influencing the outcome of cytotoxic chemo-

## WHAT IS ALREADY KNOWN ON THIS TOPIC

⇒ Clinical studies in breast cancer indicate the limited efficacy of immune checkpoint inhibitors alone, emphasizing the importance of simultaneously targeting tumor cells and immune cells. The study delves into the complexity of tumor immune microenvironment dynamics and the need for a comprehensive understanding to optimize combination immunotherapies for personalized treatment.

## WHAT THIS STUDY ADDS

⇒ This work showcases the patient-derived explant culture (PDEC) model's efficacy for mechanistic studies drug effects on the tumor immune microenvironment. The PDEC model retains the immune composition of primary breast tumors, and these resident immune cells may be activated to evaluate the antitumor response of compounds. Importantly, we can simultaneously quantify cell death of tumor cells and immune cell subtypes, possibly predicting drug-induced lymphopenia. The study reveals metformin's capacity to induce dendritic cell (DC) maturation, subsequently prompting CD4+T cell proliferation.

## HOW THIS STUDY MIGHT AFFECT RESEARCH, PRACTICE OR POLICY

⇒ By revealing the role of metformin in promoting DC maturation through Complex I inhibition, the study suggests a potential strategy to enhance immunotherapy treatments. This insight could influence the development of combination therapies that leverage the immunomodulatory effects of metformin to improve treatment outcomes.

targeted therapies which were not meant to, or do not affect immune cells directly. While the release of tumor antigens by tumor toxic compounds could trigger a beneficial

immune response,<sup>3,4</sup> the drug toxicity also targets mitotically active immune cells with potentially negative effects on antitumor immune responses.<sup>5,6</sup> Furthermore, chemotherapy-induced immunogenic cell death can, in certain circumstances, act as a trigger for the recruitment of pro-tumor macrophages,<sup>7</sup> which can reduce the sensitivity of cancer cells to paclitaxel, etoposide, and doxorubicin.<sup>8</sup>

Recent clinical studies in breast cancer (BC) have also shown that targeting the immune system through the PD-1/PD-L1 pathway alone is not effective,<sup>9–11</sup> whereas a combination of paclitaxel+anti-PD-L1, designed to target the tumor and the TIME simultaneously, has provided clinical evidence of efficiency to support approval.<sup>12,13</sup> In fact, the concept of targeting tumor cells and immune cells simultaneously is so widely tested as a treatment modality for different cancer types that nearly 90% of current PD-1/PD-L1-targeted trials include a combination therapy.<sup>14</sup>

These notions highlight that defining anticancer drug effects on not only tumor cells, but also on the TIME is crucial to understand how the drug's action translates into efficacy in the context of a heterogeneous tumor microenvironment. A better understanding of which immune cell types are activated, depleted, or otherwise impacted under the treatment, would provide important clinical trajectories, especially for a choice of the right combination of immunotherapies in a personalized treatment setting.<sup>15,16</sup> Synthetic lethality (SL) is a concept that describes the selective killing of cancer cells that harbor specific alterations of an oncogenic or tumor suppressor pathway, with a drug that is toxic to cancer cells due to specific drug-sensitizing mutations, but is much less toxic to normal cells that are lacking the mutations.<sup>17</sup> The MYC gene is amplified, or the MYC-encoded protein is elevated through other mechanisms, in up to 70% of human cancers.<sup>18</sup> The elevated or deregulated MYC levels drive many oncogenic processes, including metabolic reprogramming and non-stop cell cycle progression, but MYC also sensitizes cells to diverse inducers of extrinsic or intrinsic programmed cell death pathways.<sup>19–22</sup> These early findings have laid the conceptual foundation for MYC-dependent SL (MYC SL) therapeutic strategies, which seek to specifically harness MYC-generated vulnerability pathways as opposed to drugging the MYC protein directly.<sup>23–25</sup> A previous study exploring therapeutic opportunities through the MYC SL concept revealed that in several mouse models of MYC high BC, the MYC-high tumors in vivo are specifically vulnerable to combination treatment with venetoclax and metformin. Venetoclax is a BH3-mimetic that blocks the anti-apoptotic B-cell lymphoma-2 (BCL-2) protein<sup>26</sup> and metformin is a commonly prescribed drug for type 2 diabetes.<sup>27</sup> In particular, the treatment of syngrafted Wap-Myc tumors in mice with the venetoclax+metformin (VeM) combination results in cessation of tumor growth and the addition of anti-PD-1 checkpoint inhibitor to the treatment regimen results in a persistent treatment response—with no tumors growing in the mice even after drug withdrawal. While these

observations are consistent with the idea of immunogenic cell death as a mechanism of VeM in vivo, emerging evidence also suggests an important immunomodulatory function for metformin; it can maintain high cytotoxic T lymphocyte (CTL) activity in tumor cells<sup>28</sup> through enhancing the anti-apoptotic abilities of CD8+T cells and downmodulating PD-1/PD-L1.<sup>29,30</sup> Therefore, the anti-cancer effects observed with the VeM combination raises the interesting question whether metformin only acts by boosting cancer cell death, or whether it somehow modulates an immune response directly.

We previously developed a method to grow three-dimensional (3D) cultures of intact fragments of primary human patient-derived breast and BC tissue. The patient-derived explant culture (PDEC) model offers many advantages over conventional reductionist and artifact-prone cell co-culture and rodent models, and it has provided new insights into the biology of BC subtypes, as well as mechanisms of treatment regimens in the context of authentic human breast tumor tissue.<sup>27,31–33</sup> Since PDECs come directly from surgery, they contain viable immune cells. We considered that PDECs could offer a unique method to simultaneously investigate the effects of VeM on tumor cells and tumor resident immune cells in ex vivo conditions.

Here, we first show that PDECs maintain the immune composition and baseline immune activity of the primary breast tumors. In addition, we demonstrate that the cytolytic activity of PDEC-containing T cells can be activated with a direct T-cell activator, anti-CD3/CD28/CD2, but not via the PD-1/PD-L1 mechanism. Venetoclax depleted tumor-infiltrating lymphocytes in PDECs, as previously observed in mice,<sup>34</sup> an effect that was not counteracted by metformin. However, we report that metformin surprisingly promotes human dendritic cell (DC) maturation by altering the immune cell metabolism through the inhibition of respiratory complex I (CI). The metformin-induced DC maturation can trigger CD4+T cell proliferation, suggesting the inhibition of CI or other sites of mitochondrial respiration as a potential new therapeutic strategy to enhance immunotherapy.

## RESULTS

### PDECs maintain the immune contexture and baseline immune activity of the primary breast tumor

To define whether PDECs preserve components of the primary TIME, we investigated the presence of CD45+leukocytes in the tumor explant cultures using confocal immunofluorescence microscopy. The analysis of explants from five different patients after 3 days of ex vivo culture showed the presence of CD45+leukocytes in all studied cultures (figure 1A). To determine how well PDECs recapitulate the immune cell composition of the primary tumor sample, a workflow was designed to compare the general composition of tumor-infiltrating leukocytes (TILs) of primary tumors, with their corresponding PDECs up to 1 week in culture (figure 1B). First,

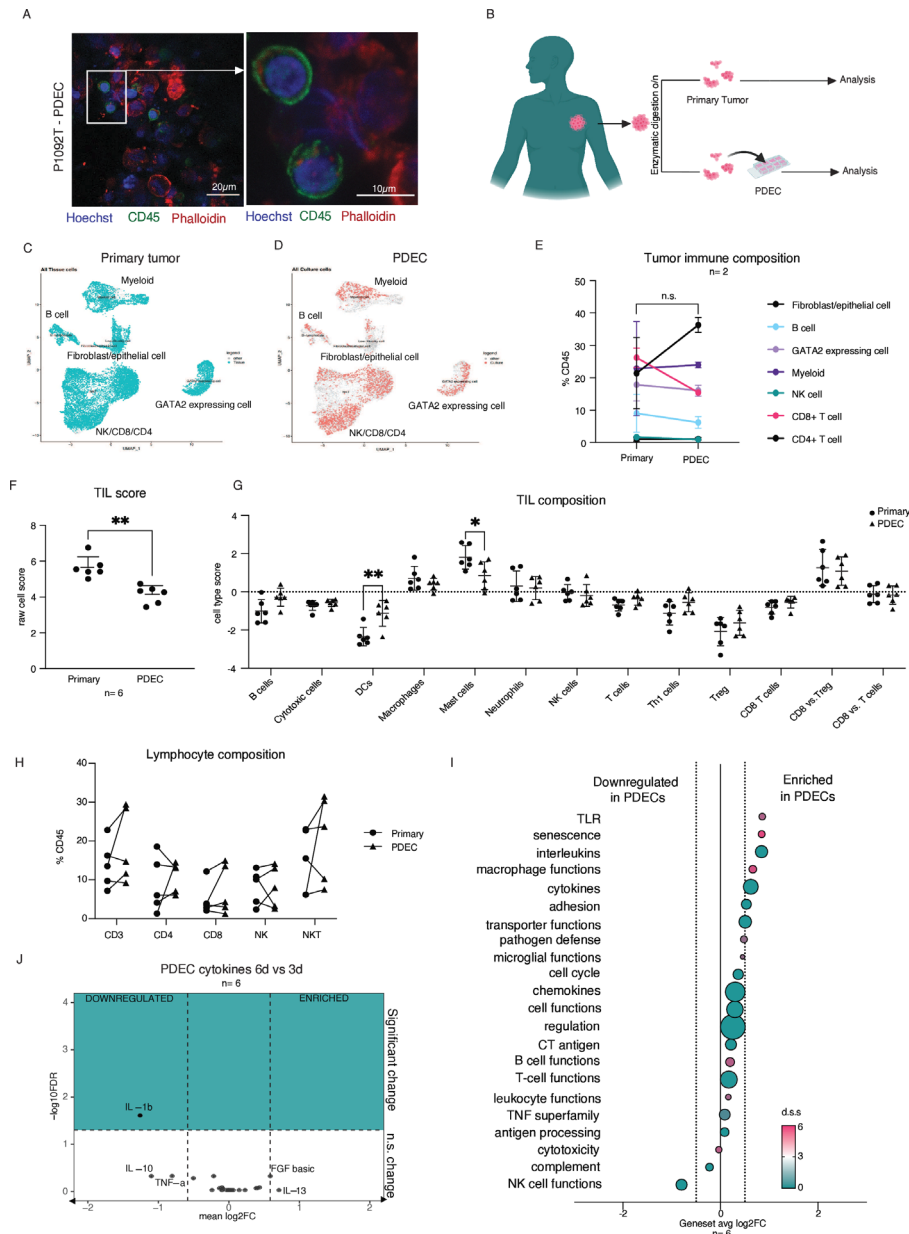


**Figure 1** PDECs maintain the immune contexture and baseline immune activity of primary breast tumor. (A) Immunofluorescent staining of CD45 and F-actin in PDECs after 72 hours in culture. P1092T refers to a tumor sample from patient 1092. (B) Schematic representation of workflow comparing primary tumor tissue to cultured tumor tissue (PDEC). (C) Single-cell RNA sequencing UMAPs after data integration from n=2 primary tumors, (D) and the corresponding PDECs. (E) Immune cell composition of primary tumors compared with the two corresponding PDECs. No significant changes were detected between any immune subtypes using the MASC algorithm (F) gene expression profiling of leukocytes of biologically independent primary tumors and their corresponding PDECs shows a decrease in TIL gene expression ( $p=0.0013$ ) after 72 hours in culture ( $n=6$ ). Statistics were done with paired t-test with two-tailed p value. (G) Immune cell composition obtained from gene expression profiling of samples from (F) normalized to nSolver tumor infiltrating leukocyte gene signature. Dendritic cell ( $p=0.0032$ ) and mast cell ( $p=0.0481$ ) numbers were significantly affected in culture. Statistics are two-way analysis of variance with Sidaks multiple comparison test. (H) Flow cytometry analysis of CD3+T cells, CD4+T helper cells, CD8+T effector cells, NK, and NKT cells from primary tumors and corresponding PDECs ( $n=8$ ) with no significant differences between primary tumor and PDECs (I) estimation of immune cell activity pathways from NanoString gene expression profiling normalized to TIL numbers. The pink fuchsia color indicates directional significance (t-statistic for each gene against each covariate) pathways considered significantly different are those with an average log2fold change of  $>0.5$  in addition to statistically significant overexpression as determined by the directional significance score above 0. (J) Cytokine profiling of explant media at 72 hours, and 144 hours. Cytokines below  $-0.58$  log2FC are downregulated more than 1.5-fold, and those with  $-\log_{10}FDR$  of 1.3 or greater are significant. Cytokine statistics were computed with one-sample t-test for deviance from 0. P values were adjusted by the FDR method. All data are presented as mean values  $\pm$ SD. FDR, false discovery rate; IL, interleukin; NK, natural killer; NKT, natural killer T; PDEC, patient-derived explant culture; TIL, tumor-infiltrating leukocytes; TLR, toll-like receptor; TNF, tumor necrosis factor

the immune cell composition of two donors was analyzed using single-cell RNA sequencing of sorted CD45+leukocytes comparing primary tumor material to explants grown for 1 week. The results demonstrated that myeloid cells, B cells, NK (natural killer) cells, CD8+T cells, and CD4+T cells were preserved in PDECs in similar proportions as the primary tumor, with no significant differences between cell types (figure 1C–E; online supplemental figure 1A,B). Second, while NanoString nSolver Gene expression profiling at 3 days in culture revealed an overall decrease in TILs within explants (figure 1F), the composition of the TILs which includes B cells, cytotoxic cells, macrophages, neutrophils, NK cells, T cells (including Th1, regulatory T cells (Treg), and CD8+) was surprisingly similar (figure 1G). We did, however, observe a decrease in the proportion of mast cells, and an increase in the proportion of DCs (figure 1G). Third, a flow cytometric comparison of CD45+leukocytes of the primary tumors and PDECs cultured ex vivo for 1 week confirmed that the relative numbers of lymphocytes (CD4+ and CD8+ T cells, NK, Natural Killer T (NKT) cells) were not significantly altered (figure 1H).

To determine the baseline activity status of primary tumor versus PDEC TILs, the gene expression profiling samples were processed to remove systematic differences in TIL numbers, and further analyzed for cell and immune activity gene sets (figure 1I). The basal activity of pathways including NK cell functions, T-cell functions, B-cell functions, cytokines and interleukins was similar to the primary tumor sample (online supplemental figure 1C). Only a few pathways, including toll-like receptor (TLR), senescence, and macrophage functions, were significantly different but we note that their corresponding profiles consisted of a small number of genes (online supplemental figure 1D). Additionally, longitudinal cytokine profiling up to 1-week revealed a significant decrease in only one cytokine, IL-1b, while the other 26 were not significantly changed (figure 1J). These results suggest that the PDEC cultures themselves have little effect on the baseline activity of the immune cells. Overall, these results indicate that the PDEC model preserves the TIME of the primary patient tumor during a 7-day culture period.

### Resident tumor-infiltrating T cells can be activated to kill tumor cells ex vivo

The presence of CD45+cells, including cytolytic cells of both innate (NK, NKT) and acquired immunity (CD8+T cells), led us to ask whether these cells could be functionally activated. We used a commercially available soluble antibody complex, anti-CD3/CD28/CD2, which cross-links the surface ligands CD2, CD3, and CD28 on T cells to provide stimulatory and co-stimulatory signals needed for robust T-cell activation, herein referred to as anti-CD3/CD28/CD2. We compared anti-CD3/CD28/CD2 to therapeutically relevant antibodies for PD-1 and its ligand (PD-L1) (programmed death ligand 1) to detect the “maximum” T-cell response in PDECs, and to determine

whether in our PDEC model the PD-1-PD-L1-axis is a critical signaling pathway that limits the physiological activity of resident T cells.<sup>35</sup>

We treated the explants for 72 hours and measured general cell death with the CellTox green assay, observing a statistically significant increase in cell death on anti-CD3/CD28/CD2 treatment whereas no cell death was observed following treatment with anti-PD-L1 (figure 2A,B). We randomly chose three primary tumor samples from the CellTox experiment and performed multiplex immunohistochemistry (IHC) to confirm that the samples contained immune cells, and that the cell death was a result of T-cell cytotoxicity (figure 2C; online supplemental figure 2A). To further verify that any cell death seen following anti-CD3/CD28/CD2 likely came from tumor cells, we performed flow cytometric analysis of PDECs, and quantified absolute numbers of CD45–non-hematopoietic cell populations, which were mostly tumor cells, but also stromal cells like fibroblasts. Here we also observed a reduction of tumor cells after T-cell activation (figure 2D). We further stained and imaged multiple fragments within PDEC cultures of the same patient and found that immune cells are retained in the intratumoral regions evenly throughout the culture, decreasing the chance that any response is due largely due to uneven distribution of immune cells between wells (online supplemental figure 2B,C,D).

Consistent with an increase in cytotoxic activity leading to cell death, quantitative polymerase chain reaction (qPCR) analysis of PDECs following anti-CD3/CD28/CD2 treatment revealed a statistically significant increase in interferon (IFN)- $\gamma$  expression, and a trend for elevated messenger RNA (mRNA) expression of granzyme B (GZMB) and perforin-1 (PRF1) (figure 2E–H). Both PRF1 and GZMB are expressed by cytotoxic T cells and NK cells on activation, while IFN- $\gamma$  is a signature proinflammatory cytokine typically used to measure immune activation.<sup>36,37</sup> The cell death and mRNA results in response to anti-CD3/CD28/CD2, along with the fact that anti-PD-L1 monotherapy has no positive effect on tumor cell death, or the transcription of *IFN- $\gamma$* , *GZMB*, or *PRF1*, reinforce the idea that the cell death seen previously is likely a result of T cell receptor (TCR)-triggering, and the downstream effects of T-cell activation.

We profiled cytokines of T-cell activation and inflammation from PDEC supernatant after 72 hours of anti-CD3/CD28/CD2 (n=16), and anti-PD-L1 (n=6) treatments. The results highlight the ability of PDECs to reflect patient heterogeneity, while still capturing the general trend of cytokines expected after robust T-cell activation (figure 2I,J). For example, we observed an increase in interleukin (IL)-2 which is secreted by CD4+T cells on antigen stimulation, and in IL-10, which is secreted in response to immune activation by several different cell types<sup>38,39</sup> (figure 2I). In accordance with the previous qPCR findings, we observed that unlike anti-CD3/CD28/CD2 treatment, anti-PD-L1 monotherapy did not deviate far from the control, suggesting negligible effect from the

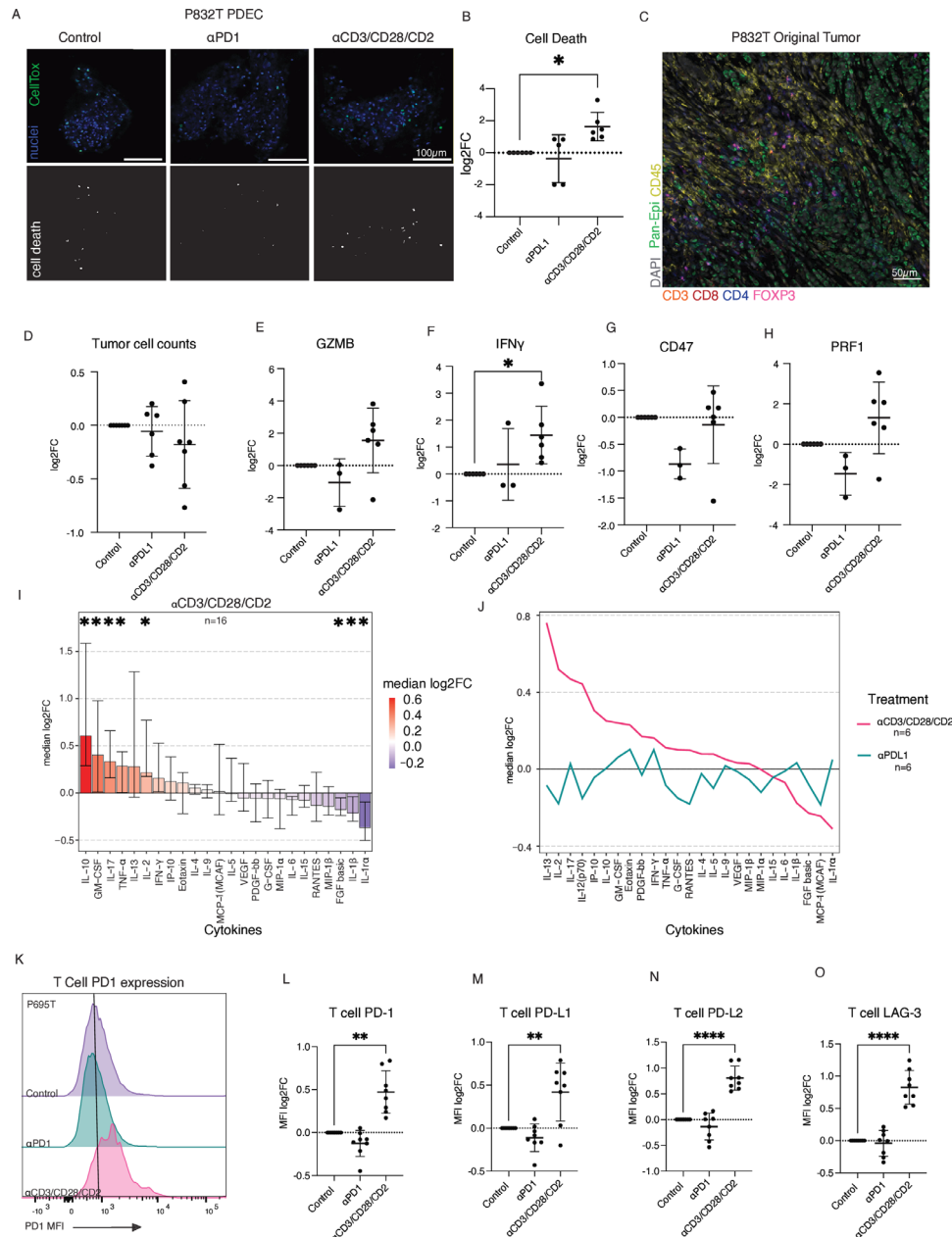


**Figure 2** Resident tumor-infiltrating T cells can be activated to kill tumor cells ex vivo. (A) CellTox staining of P832T PDEC following treatment with a-PD-1 and anti-CD3/CD28/CD2. (B) Quantification of cell death from IF images corresponding to  $n=6$  biologically independent PDECs, showing significant cell death following anti-CD3/CD28/CD2 treatment ( $p=0.0321$ ) quantified with a one-way ANOVA with Fisher's exact test. (C) Immune infiltration of primary tumor from which PDECs in figure 3A. were derived from. (D) Tumor cell (CD45<sup>-</sup>) counts in  $n=7$  biologically independent PDECs ( $n=6$  for aPD-L1) following aPD-L1 and antiCD3/CD28/CD2 treatment as the log<sub>2</sub>FC of the absolute cell numbers normalized the control (E–H) qPCR analysis of *GZMB*, *IFN-γ* ( $p=0.0208$ ), *CD47*, *PRF1* relative to the control.  $n=3$  for aPD-L1,  $n=6$  for control and anti-CD3/CD28/CD2-treated. Statistical significance was tested with a one-way ANOVA with Fisher's exact test. Data are presented as mean values $\pm$ SD. (I) Multiplex cytokine profiling of PDECs after 72 hours anti-CD3/CD28/CD2 treatment  $n=16$ . Each cytokine is tested with a one-sample non-parametric Wilcoxon test for deviance from 0 (no change) and  $p$  values adjusted by an FDR method. Cytokines are ordered by median log<sub>2</sub>FC and plotted with error bars ranging the IQR. (J) Comparison of median log<sub>2</sub>FC of cytokines between anti-CD3/CD28/CD2 and aPD-L1 treatments in PDECs  $n=6$ . (K) Flow cytometry representation of median fluorescence intensity of checkpoint marker, PD-1, on CD3<sup>+</sup>T cells in control, aPD-1 and anti-CD3/CD28/CD2-treated PDEC of P695T. (L–O) Graphs quantifying the median surface expression of T-cell checkpoint proteins relative to control. Statistical significance was tested with significant increase in PD-1 ( $p=0.0010$ ), PD-L1 ( $p=0.0096$ ), PD-L2 ( $p<0.0001$ ), and LAG-3 ( $p<0.0001$ ) in response to anti-CD3/CD28/CD2. Statistical significance was tested with a one-way ANOVA with Fisher's exact test. Data are presented as mean values $\pm$ SD. ANOVA, analysis of variance; aPD-1, anti-programmed cell death 1; aPD-L1, anti-programmed death ligand 1; FDR, false discovery rate; GZMB, granzyme B; IF, immunofluorescence; IFN, interferon; LAG-3, lymphocyte activation gene 3; MFI, median fluorescence intensity; PD-1, programmed cell death 1; PDEC, patient-derived explant culture; PRF1, perforin-1; PD-L1, programmed death ligand 1; PD-L2, programmed death ligand 2; qPCR, quantitative polymerase chain reaction.

drug in terms of induced cytokine expression (figure 2J). For T cell-specific analysis, CD3+T cells were profiled directly for signs of exhaustion following treatment by flow cytometry, measuring the median fluorescent intensity of checkpoint ligands/receptors programmed death ligand 2 (PD-L2), PD-L1, lymphocyte-activation gene 3 (LAG3), and PD-1 on the surface of the cells. Once again, anti-CD3/CD28/CD2, but not anti-PD-1, induced expression of these checkpoint molecules, suggestive of T-cell activation (figure 2K–O; online supplemental figure 2E). The transcriptional and cytokine data support the general detection of immune activation within PDEC cultures, while Immunofluorescence (IF) and flow cytometry analysis of PDECs suggest that T cells are functionally activatable to kill tumor cells ex vivo.

Together, the presence of the primary tumor TIL repertoire within PDECs and the evidence for activatable cytolytic properties in the tumor CD8+T cells demonstrate PDECs as a versatile model to study various aspects of tumor-immune tissue interactions and anticancer drug responses in the context of the TIME.

### Assessment of combination therapy with venetoclax reveals lymphodepletion of T cells

Since the PDECs preserved the TIME, we recognized an opportunity to further explore and validate the specific responses of tumor cells and TIME to the VeM combination, which shows strong in vivo antitumor activity in several mouse models of MYC-driven aggressive BC.<sup>27</sup> Clinically, venetoclax has been observed as a lymphodepleting agent as it induces apoptosis in BCL-2 reliant subsets of T cells.<sup>34</sup> The lymphodepleting activity is a potential clinical concern, as it could negatively impact immune system functions and reduce the opportunities to combine venetoclax with immune-modulating therapies. We first tested the idea that metformin component of VeM perhaps affords protection to immune cells against the lymphodepleting actions of venetoclax, which could explain the better in vivo effect of VeM in comparison to single treatments.<sup>27</sup> In parallel with VeM, we treated PDECs with clinically relevant paclitaxel, a chemotherapy used to treat primary breast tumors, often in combination with other drugs (figure 3A).

Unsupervised clustering of cytokines of 10 patient samples revealed tight clustering by treatment. We observed a consistent downregulation of most T-cell-associated cytokines (as determined in figure 2I) in response to VeM, irrespective of MYC-status, suggestive of a depletion of lymphocytes (figure 3B, online supplemental figure 3A). Flow cytometry analysis of CD45-cells, mainly tumor cells, showed some variation in the level of apoptotic responses to VeM between independent PDEC samples (figure 3C,D), whereas every VeM-treated sample showed a noticeable drop in the number of CD4+ and CD8+ T cells, with a more significant decrease in the numbers of CD8+T cells (figure 3E,F). Although we failed to see tumor cytotoxicity in PDECs after paclitaxel treatment, likely due to a delay between the drug's

primary and secondary modes of action ex vivo,<sup>40</sup> we did notice an increase in inflammatory cytokines suggestive of inflammation (IL-2, IL-10, IL-4, IL-15) from a subset of patients. We took a transcriptional approach to broaden the variety of immune cell types we could observe simultaneously (figure 3G). As with the cytokine profiling and flow cytometry, we noticed a clear diminishing impact of VeM on T cells. These results led us to refute the initial working hypothesis suggesting that metformin protects BCL-2-reliant CTLs against the lymphodepleting effects of venetoclax since none of our experiments supported this notion.

### Metformin contributes to dendritic cell activation ex vivo and in vivo

The fact that metformin did not protect T cells from apoptosis following venetoclax treatment led us to hypothesize that the immunogenic benefits of metformin might derive from the immune cells that were spared within the PDEC tumor microenvironment; for example, DCs, macrophages, and NK cells remained unchanged (figure 3G). We looked into the gene expression profiles of VeM-treated explants from four patients, and found that many of the overexpressed genes, including *HMGB1*, *CD97*, *MAF*, and *LAMP-3*, could be attributed to the activation of antigen-presenting cells (figure 4A). A similar profile was observed for VeMA-treated patients, but not either paclitaxel or paclitaxel+anti-programmed death ligand 1 (aPD-L1) (online supplemental figure 4A–C). A metascape analysis of the most significantly affected biological pathways following VeM treatment based on the overexpressed genes included: cytokine signaling in the immune system, adaptive immune response, and regulation of mononuclear cell proliferation—suggesting that even with the depletion of T cells, there were still elements important for T-cell response being upregulated (figure 4B). These observations combined with an increase of macrophage-inflammatory protein 1-beta, and IL-17 which are secreted by innate lymphoid cells and monocyte-derived cells (figure 4C), and the elevated expression of LAMP-3 on a larger set of patient samples (online supplemental figure 4D), suggested we focus our investigation on the antigen-presenting cells.

In agreement with our gene expression profiling (figure 3G), we also did not detect a change in the number of antigen-presenting cells (APCs) following venetoclax, metformin, or VeM treatment with flow cytometry (online supplemental figure 4E). However, with established surface marker panels for APCs,<sup>41–42</sup> we found that metformin clearly increased the proportion of APCs with a potentially more DC-like phenotype (CD11c+, human leukocyte antigen-DR isotype (HLA-DR)+, CD14-) (online supplemental figure 4F,G), which expressed increased levels of CD86 following metformin treatment, hinting that metformin activates these cells (online supplemental figure 4I). To ensure these cells are more likely to be DCs than macrophages, we repeated the experiment with markers of DCs and DC activation,

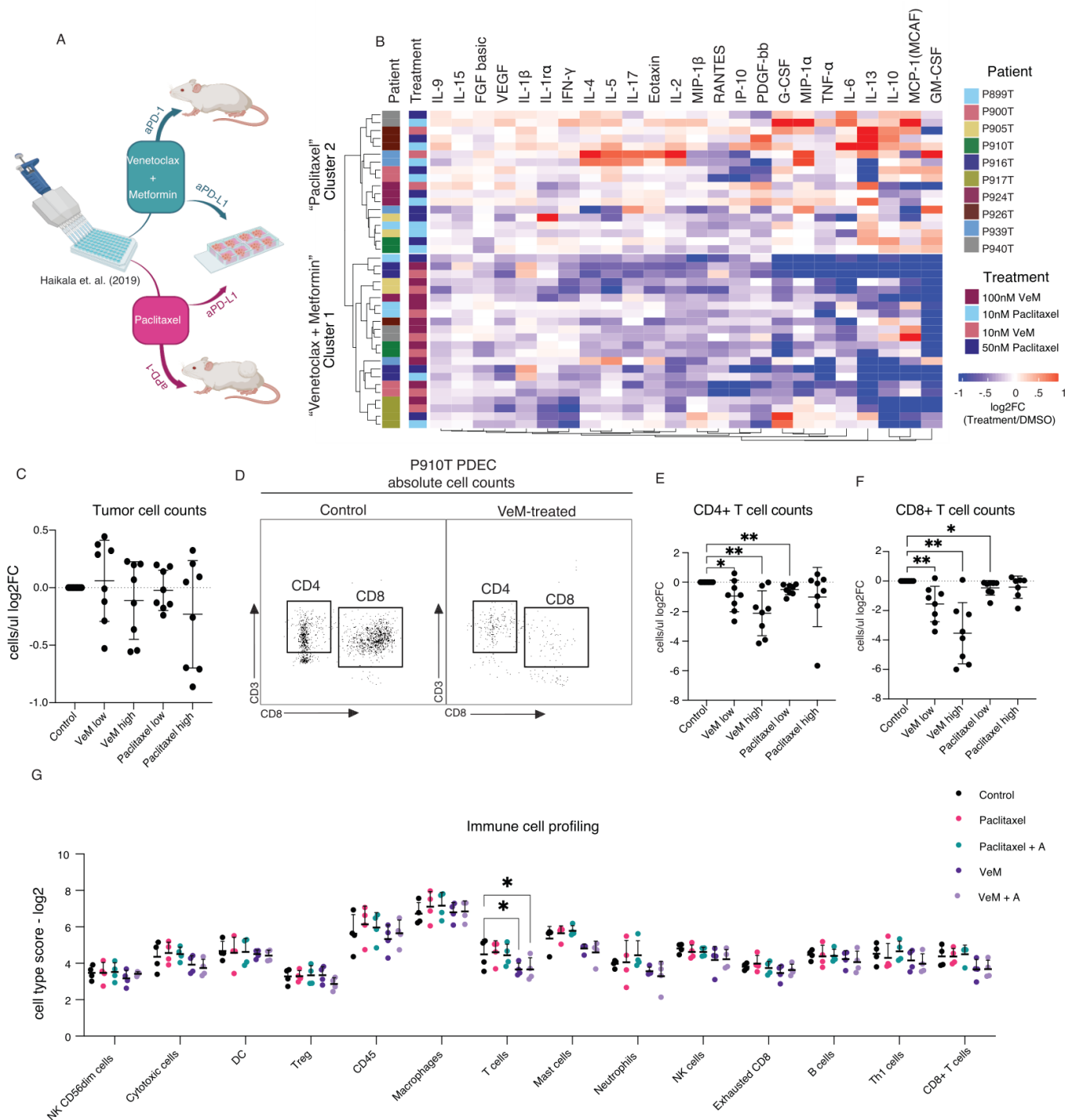


**Figure 3** Assessment of combination therapy with venetoclax reveals lymphodepletion of T cells. (A) Schematic summary of the previous finding<sup>27</sup> in WAP-Myc mouse model of MYC-driven breast cancer where venetoclax+metformin+aPD-1 treatment in mice resulted in durable antitumor immunity. Here, the VeM treatment along with paclitaxel was profiled in PDECs. (B) Unsupervised hierarchical clustering (Euclidean distance, complete linkage) of PDECs based on cytokine secretion following venetoclax+metformin and paclitaxel treatments (n=10 biologically independent PDECs). (C) CD45<sup>-</sup> tumor cell viability after VeM or paclitaxel treatments (D) a representative image of quantifying cell viability through flow cytometry for panels (E–F) (E) low (10nM venetoclax+10mM metformin) (p=0.0428) and high (100nM venetoclax+10mM metformin) (p=0.0059) concentrations of VeM negatively impact CD4 T cell viability (CD45<sup>+</sup>CD3<sup>+</sup>CD56<sup>-</sup>CD4<sup>+</sup>) (F) low (p=0.0082) and high (p=0.0019) concentrations of VeM negatively impact T effector (CD45<sup>+</sup>, CD3<sup>+</sup>, CD56<sup>-</sup>, CD8<sup>+</sup>) viability (G) NanoString gene expression profiling of projected cell type scores following treatment of n=4 biologically independent PDECs. High VeM (100 nM venetoclax+10 mM metformin) p=0.0434) without and with aPD-L1 (p=0.0449) negatively impact the T-cell score. Statistical significance was tested with a two-way analysis of variance with Fisher’s LSD. All data are presented as mean values $\pm$ SD. aPD-1, anti-programmed cell death 1; aPD-L1, anti-programmed death ligand 1; DC, dendritic cell; DMSO, dimethyl sulfoxide; LSD, least significant difference; NK, natural killer; PDEC, patient-derived explant culture; Treg, regulatory T cell; VeM, venetoclax+metformin.



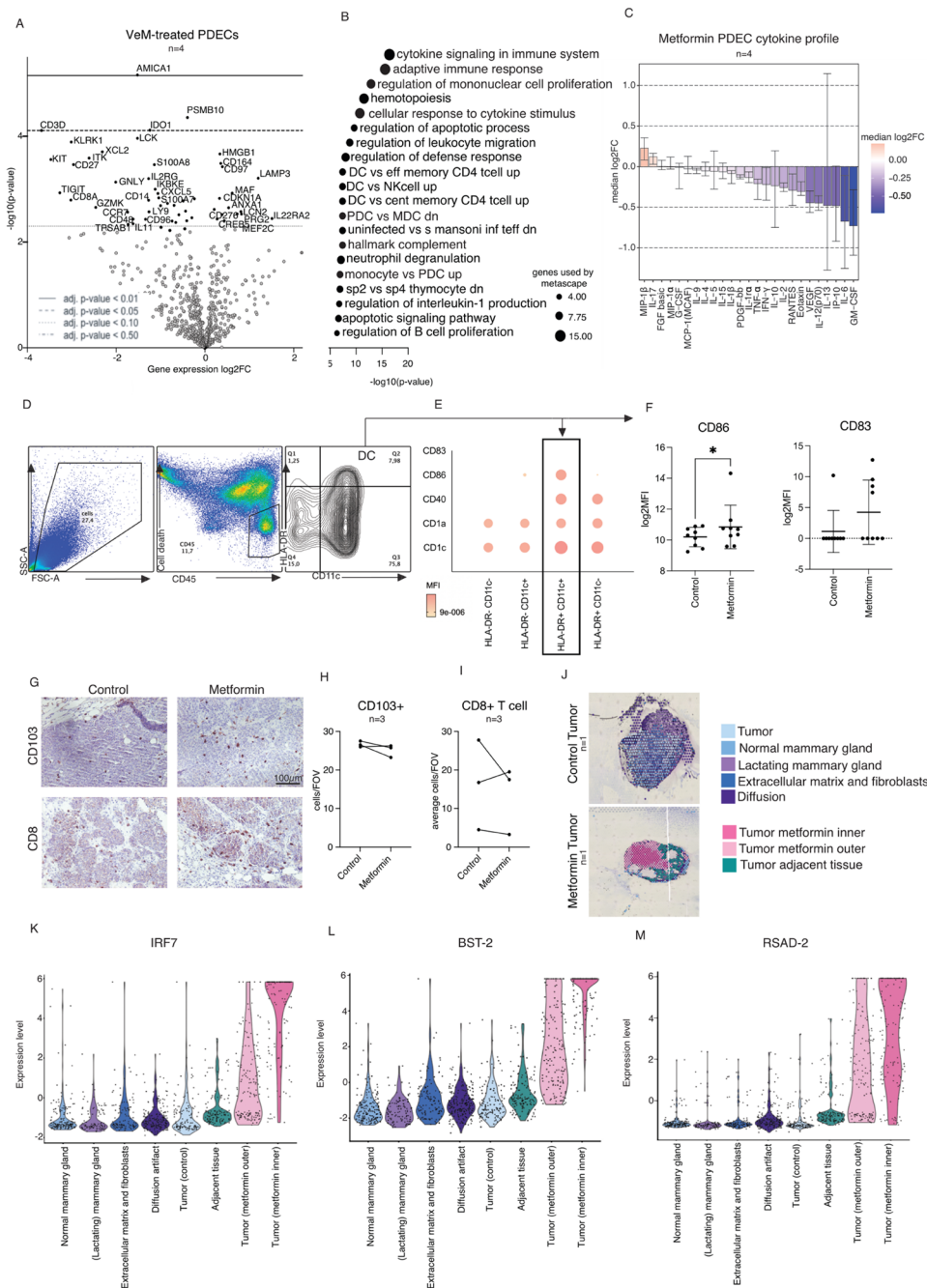


**Figure 4** Metformin contributes to dendritic cell activation ex vivo and in vivo. (A) Volcano plot of differentially expressed genes of  $n=4$  venetoclax+metformin-treated PDECs. Adjusted p value key described on the plot. (B) Metascape analysis of differentially expressed genes from (A) which are at least 20% upregulated and significant with a p value of  $<0.05$ . The graph depicts terms which were significantly enriched after treatment. Ball size corresponds with the number of genes that overlapped with the gene signatures tested on metascape. (C) Cytokine profiling of PDECs following 10mM metformin treatment. Each cytokine was tested by one-sample non-parametric Wilcoxon test for deviance from 0 (no change) and p values adjusted by FDR method  $n=4$ . (D) Flow cytometry gating of quadrants with varying expression of HLA-DR and CD11c and (E) the median fluorescence intensity of markers CD1c, CD1a, CD40, CD86 in these four quadrants to determine select antigen-presenting cells with a DC phenotype. (F) CD86 and CD83 expression of dendritic cells following metformin treatment (G) Representative immunohistochemistry staining of CD103 dendritic cell activation marker and CD8 cytotoxic T-cell marker in control and metformin-treated Wap-Myc mouse tumors ( $n=3$  control, and  $n=3$  metformin-treated mouse tumors). (H–I) Quantification of (G). (J) Control and metformin-treated mouse tumors from Wap-Myc mice with spatial annotations of tissue areas. Each circle is 10  $\mu$ m in diameter. (K–M) Mouse DC activation markers, *Bst2*, *Irf7*, and *Rsad2* in varying tumor regions as shown in (J). All data are presented as mean values  $\pm$  SD. Statistical significance was tested with a one-way analysis of variance with Fisher's exact test. DC, dendritic cell; FDR, false discovery rate; FOV, field of view; HLA-DR, human leukocyte antigen-DR isotype; MFI, median fluorescence intensity; MDC, myeloid dendritic cell; MFI, median fluorescence intensity; MDC, myeloid dendritic cell; Nk, natural killer; PDEC, patient-derived explant culture; PDC, plasmacytoid dendritic cell.

and found that markers including CD1c, CD1a, CD40, and CD86 could be observed on the surface of the HLA-DR+CD11c+high-expressing cells (figure 4D,E, online supplemental figure 5A). We identify these cells as DCs, although the panel of markers is too limited for definite identification of this cell type. Analysis of these DCs revealed a significant increase in CD86 expression, suggestive of DC activation. Moreover, samples that did not express CD83 began to express DC maturation marker CD83 following metformin treatment (figure 4F). The DC modulation could have positive implications for antitumor immunity, since the predominant role of DCs is to activate T cells, while macrophages clear apoptotic cells and microbes through phagocytosis. Therefore, both the metformin-induced transcriptomic activation of DC activation markers and the increase in the proportion of DC-like cells within the APCs (online supplemental figure 4F,G) were consistent with the idea that metformin could play a role in human DC activation, a notion which has not been made prior to the present study. The remaining APCs, consisting of monocytes and macrophages referred to as mono-macs (CD11c+, HLA-DR+, CD14+), also exhibit a significant decrease in markers associated with immunosuppressive M2 macrophages (online supplemental figure 4F,H) in corroboration to previous mouse studies and human in vitro co-culture studies,<sup>43–45</sup> which we now extend to authentic ex vivo human tumor tissue cultures.

To explore the effects of metformin in vivo, we investigated Wap-Myc tumor samples from metformin-treated mice for conventional DC (CD103+) and CD8 T cell (CD8+) numbers but found no significant changes in the cells expressing either marker (figure 4G,H,I). These findings were consistent with our findings in PDEC-TIME, where there was an increase in APC activation, but not in overall numbers. Spatial 10x Genomics profiling of Wap-Myc mouse tumor tissue from metformin-treated animals revealed enriched DC activation in metformin-treated mouse compared with control mouse material as determined by the gene expression profiles; metformin increased *Irf7*, *Bst2*, and *Rsad2* expression, while macrophage marker, *CD68*, expression was downmodulated (figure 4J–M; online supplemental figure 5B). Details of how the 10x Genomics and how the tumor areas were classified are explained in supplementary (online supplemental figure 6A). The results from human explants and mouse tumor tissue, treated with venetoclax and metformin (alone or in combination) together suggest that specifically metformin, and not venetoclax, affects DC activation, without altering their numbers.

### The mitochondrial respiratory complex I regulates DC activation and DC-mediated activation of CD4+ T-cell proliferation

To determine whether metformin activates APCs directly or through heterotypic cellular interactions, we isolated monocytes from human peripheral blood mononuclear cells (PBMC) of healthy donors. The PBMC-derived

monocytes were then differentiated into either macrophages or DCs. Flow cytometric analysis of macrophages showed that metformin decreased the surface expression of CD163 and CD206 on macrophages differentiated from monocytes with macrophage colony-stimulating factor (M-CSF), markers commonly associated with immunosuppressive macrophages, corroborating publications with similar findings (figure 5A–D).<sup>44–46</sup> RNA bulk sequencing of metformin-treated monocyte-derived DCs from six donors showed clear evidence for an increase in DC activation (figure 5E, online supplemental figure 7A). Additionally, flow cytometry analysis of monocyte-derived DCs revealed that treatments containing metformin induced a higher proportion of CD86-high, HLA-DR-high activated DCs from the total population (figure 5F,G) suggesting that metformin indeed directly contributes to DC activation. Flow cytometry analysis of DC surface activation markers, and a transcriptional increase in DC activation gene sets suggests a less documented role of DCs as a potential mediator of metformin's antitumor effect in humans.

Metformin is a medicinal biguanide, which acts as a weak inhibitor of mitochondrial respiratory CI (figure 5E).<sup>47</sup> Inhibition of CI decreases the generation of ATP from oxidative phosphorylation (figure 5E–H, online supplemental figure 8A–C) and the resulting increase in AMP:ATP and ADP:ATP ratios activate adenosine 5'-monophosphate kinase (AMPK), an event commonly observed in metformin-treated cells in vitro and in vivo.<sup>48–49</sup> To test whether metformin induces DCs activation through activation of AMPK or inhibition of the mitochondrial CI, an experiment was designed to evaluate separately the effect of AMPK-activation, and CI inhibition on DC activation. We found that inhibition of mitochondrial CI with metformin, with the classical CI inhibitor rotenone or with a specific ubiquinone reduction site targeted CI inhibitor IACS-010759<sup>50</sup> led to an increase in DC activation, whereas direct pharmacological allosteric AMPK activator A-769662 had no noticeable effect (figure 5I). These results suggest that the mechanism by which metformin activates DCs is largely through CI inhibition.

DCs which express elevated levels of activating co-stimulatory signals, including CD86, promote T-cell proliferation and acquisition of their cytotoxic abilities.<sup>51</sup> Thus, we explored whether metformin's effect on DC activation has functional consequences on the activation of T cells. We pretreated DCs with metformin, A-769662, IACS-010759 and rotenone for 48 hours, and then co-cultured the DCs with autologous T cells in the absence of drugs. Importantly, we used anti-CD3 in the co-culture to fulfill the requirement of T cells to not only receive secondary co-stimulatory signals from APCs, but also to have the primary signal through the T-cell receptor which we were supplementing artificially (online supplemental file 8). An increase in CD4+T cell proliferation was quantified as a shift in the proportion of T cells in proliferation (G0=unproliferated T cells, G1=first division, etc),

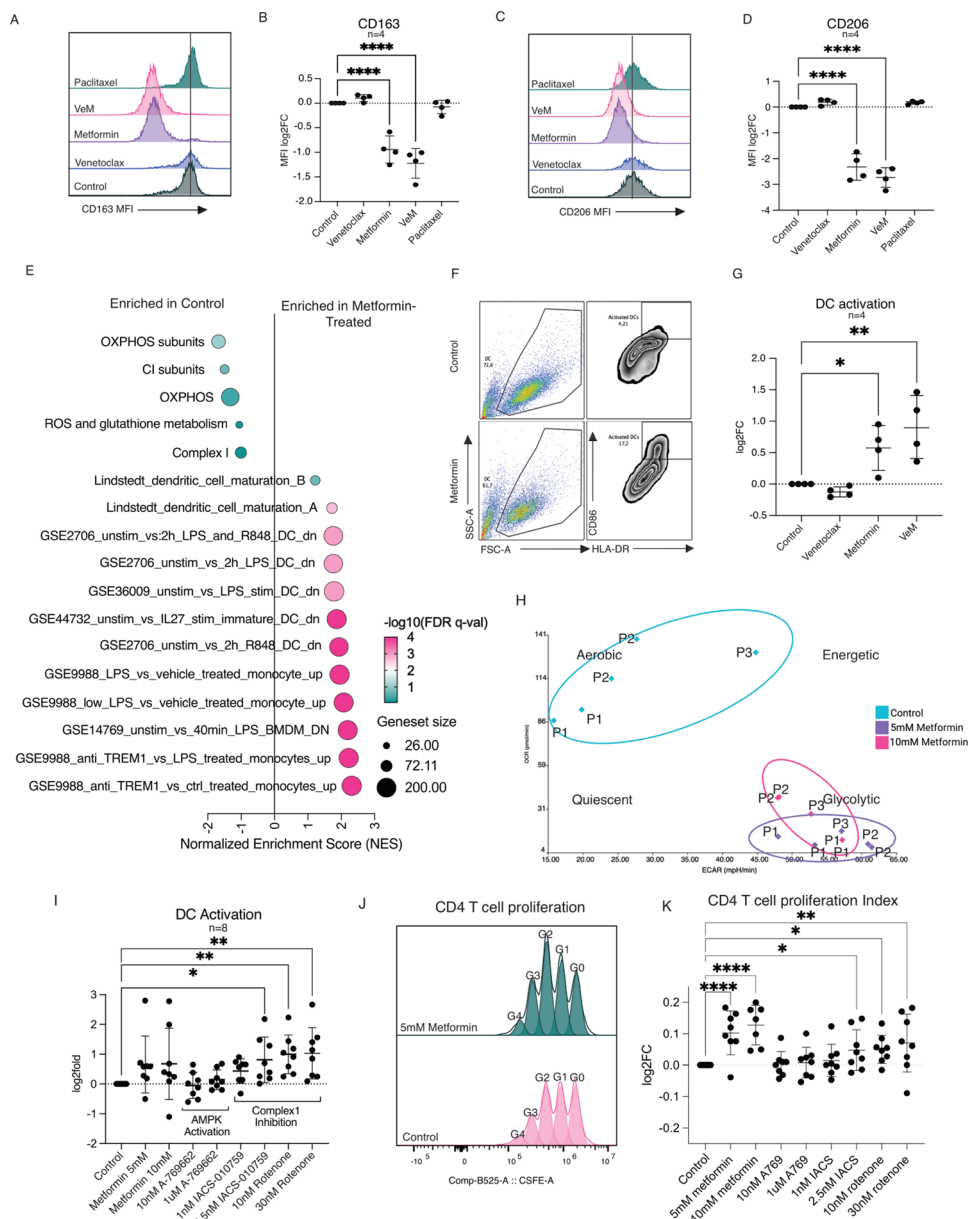


**Figure 5** Complex 1 inhibition contributes to DC activation and CD4+T cell proliferation. (A) Representative flow cytometry histogram of median fluorescence intensity of CD163 of monocyte-derived macrophages following treatment. (B) Quantification of (A) from monocyte-derived macrophages of four biologically independent PBMC donors. (C) Representative flow cytometry histogram of median fluorescence intensity of CD206 of monocyte-derived macrophages following treatment. (D) Quantification of (C) from monocyte-derived macrophages of four biologically independent PBMC donors. (E) Gene Set Enrichment Analysis comparison of differentially expressed genes between 10 mM metformin and control-treated PBMC-derived dendritic cells from  $n=6$  biologically independent PBMC donors. (F) Flow cytometry gating guide of HLA-DR and CD86 high-expressing DCs which are referred to as “activated DCs”. (G) Quantification of the percentage of activated DCs following treatment from  $n=4$  monocyte-derived DC samples with significant increase in surface expression of CD86 and HLA-DR following metformin ( $p=0.0226$ ) and venetoclax+metformin ( $p=0.0014$ ) treatments (H) seahorse extracellular flux assay of monocyte-derived DCs ( $n=3$ , referred to as P1, P2, P3). Data points with the same label are technical repeats. Data shows that 24 hours metformin treatment shifts the energy requirements of DCs from aerobic to glycolytic. (I) Quantification of DC activation following a larger panel of treatments with significant DC activation following 2.5 nM IACS-010759 ( $p=0.0287$ ), 10 nM rotenone ( $p=0.0105$ ), and 30 nM rotenone ( $p=0.0309$ ) (J) representative T-cell proliferation plot. G0 refers to the undivided generation, with each increasing G number referring to the number of proliferative cycles (K) flow cytometry analysis of CD4+T cell proliferation index indicating the proportion of the proliferating samples that keep proliferating (G1–G4) with significant increases in CD4+T cell proliferation following 5 mM metformin ( $p=0.0043$ ) and 10 nM rotenone ( $p=0.0161$ ) treatments. All data are presented as mean values  $\pm$  SD. Statistical significance was tested with a one-way analysis of variance with Fisher’s exact test. DC, dendritic cell; FDR, false discovery rate; FSC-A, forward scatter area; GSEA, gene set enrichment analysis; HLA-DR, human leukocyte antigen- DR isotype; MFI, median fluorescence intensity; PBMC, peripheral blood mononuclear cells; PDEC, patient-derived explant culture; SSC-a, side scatter area.

or in other words, the number of divisions of already-proliferating cells (figure 5J–K). This biologically relevant “proliferation index” clearly showed that the trend in CD4+T helper cell proliferation mirrored the trend in DC activation (figure 5K), suggesting increased co-stimulation of these already-dividing cells. Meanwhile, the “division index”, which is a measure of the total proportion of cells that begin to divide (the ratio of G1-4 to G0), revealed a significant negative impact on overall CD4+T cell proliferation following co-culture with DCs treated with AMPK-activator, A-769662 (online supplemental file 8). This can be a result of AMPK-activation interfering with DC maturation as seen in mice.<sup>52</sup> The highest dose of metformin negates the increase in overall T-cell proliferation induced by 5 mM metformin, likely due to the increase of metformin’s many modes of action which includes AMPK-activation. An increase in overall proliferating T cells is seen with direct CI inhibition using 10 nM and 30 nM rotenone, suggesting that CI inhibition may also be behind the reason we see an increase with 5 mM metformin. These data suggest that CI inhibition may improve an antigen-specific immune response through the activation of DCs.

## DISCUSSION

The importance of targeting tumor cells and exploiting the TIME simultaneously is evident in the increasing number of clinical trials combining targeted therapies or chemotherapies with immunomodulatory compounds.<sup>53</sup> However, microenvironmental interactions and heterogeneity within the tumor microenvironment that affect treatment response,<sup>54–56</sup> can be difficult to model in the laboratory. In vivo, animal models may require surrogate, species-specific reagents with different pharmacological properties than the original therapeutic drug. In vitro, organoid models capture disease heterogeneity and tumor intrinsic features to some extent but are lacking most immune cell components.<sup>57–59</sup> Some organoid models are being adapted, for example, to use autologous primary tumor-specific CD8+T cells to screen tumor cell killing in response to increased drug-induced T-cell cytotoxicity.<sup>60</sup> Although beneficial in terms of throughput, this is limited to CD8+T cell-mediated cytotoxicity. Moreover, using the tumor itself is crucial because antitumor T-cell responses can be tumor site specific, even within the same patient.<sup>61 62</sup> So, while peripheral blood can be powerful as a predictor of monitoring clinical outcome,<sup>63</sup> tumor resident immune cells can be more informative for drug development by capturing the complex tumor-TIME dynamics which can be shaped by the baseline immune composition.<sup>64</sup> Indeed, there is a clear correlation with the full TIME repertoire and clinical outcome, prompting more attention to models with a more diverse repertoire of autologous tumor immune cells.<sup>65–68</sup>

Here we explored the opportunities provided by BC PDECs. While organoids can be considered as “reconstruction” models where tumors are dissociated into single

cell components that form new structures, explants are a “deconstruction” of the tumor which capture elements of the original architecture, heterogeneity, and immune cell composition of the tumor—but in smaller pieces. Earlier works show that human ex vivo explants from various cancer types retain tumor and stroma components in addition to autologous immune cell populations and can respond to anti-PD-1 depending on the cancer type.<sup>35 69 70</sup> We deduced through single-cell sequencing, gene expression profiling, flow cytometry, and cytokine profiling of PDECs in comparison to primary tumor material that PDECs also retain all major immune cell subtypes and baseline immune cell activity up to 1 week in culture, which makes these PDEC-TIME cultures an attractive model to explore tumor-TIME dynamics, although this specific model is not optimized for stromal interactions, as these are disrupted during the enzymatic processing of the samples.

While we failed to see an increase in T-cell activity or tumor cell death in BC PDECs in response to either anti-PD-1 or anti-PD-L1, we did see strong immune activation in response to artificial T-cell activation using an anti-CD3/CD28/CD2 tetramer similarly to Voabil (2021), suggesting that T cells within breast tumors lack tumor antigen reactivity. In response to anti-CD3/CD28/CD2, we first observed cell death appearing in PDECs with CellTox staining and an increase in immune activation markers IFN- $\gamma$ , PRF1, and GZMB via qPCR from bulk RNA. Subsequent flow cytometry and cytokine profiling revealed that the cell death was specifically affecting CD45<sup>+</sup> tumor cells, while cytokines of T-cell activation (eg, IL-2, IFN- $\gamma$ , interferon gamma-induced protein 10 (IP-10)) were increased along with T-cell surface expression of checkpoint molecules like PD-1, PD-L1, PD-L2, and LAG-3. Altogether, these findings suggest that with the correct treatment strategy, breast tumor-resident immune cells in PDECs have the potential to be exploited for preclinical antitumor activity.

In our previous work on MYC-driven mouse models of BC, we observed exceptionally durable tumor growth control following a triple-treatment of VeM, and anti-PD-1.<sup>27</sup> The ex vivo PDEC model, however, revealed a downregulation of all 27 tested cytokines following VeM treatment. Additional flow cytometry data revealed severe T-cell toxicity, especially among CD8+T cytotoxic cells. We attributed this phenomenon to corroborating the lymphotoxic effects of venetoclax on human T cells observed in vitro and in vivo.<sup>34 71</sup> Nevertheless, gene expression profiling of a larger repertoire of immune cells revealed that other immune cell subsets were unaffected by VeM in terms of numbers, and that there was a significant increase in genes and cytokines suggestive of APC-activation. The survival and activation of APCs, including macrophages and DCs, is highly interesting since APCs are known to mold the pro-/antitumor properties of TIME, and thus play a role in the efficacy of immune-checkpoint blockade.<sup>72 73</sup>

Classically activated “M1-like” proinflammatory macrophages have been suggested as a standalone therapeutic

strategy for BC due to their tumoricidal properties,<sup>74</sup> and a biomarker of increased survival in response to trastuzumab.<sup>75</sup> Meanwhile, alternatively activated “M2-like” macrophages have been linked to poor prognosis in BC. Metformin has been shown to prevent M2 polarization of macrophages, induce M1 polarization of macrophages, and increase the efficacy of checkpoint inhibition in human and mouse studies.<sup>44–46 76 77</sup> Extending the previous results, we demonstrate in PDECs that 5 mM–10 mM of metformin directly decreases the proportion of immunosuppressive CD163+M2like macrophages.

DCs are highly potent APCs that can trigger robust, antigen-specific T-cell activation *in vivo* on maturation, and their increased presence is generally considered a good prognostic marker in BC.<sup>78 79</sup> Our data show that while metformin does not influence the total number of APCs, it induces a higher proportion of activated DCs in PDECs, and we also observed that metformin promotes DC activation of isolated DCs from human PBMCs. Thus, our data suggests that metformin has a direct DC-activating function, contrary to the idea that DC activation was solely induced through the release of tumor antigens following VeM treatment.

Metformin acts as a weak inhibitor of mitochondrial respiratory CI<sup>47</sup> and as an AMPK-activator.<sup>48 49</sup> To investigate how metformin mediates its DC activating function, we explored these two most well-known mechanisms of metformin action. We only observed that the metformin effects on DC activation were phenocopied by respiratory complex I inhibition (CI-i), but not by direct allosteric activation of AMPK. Previous reports have suggested that CI-i of DC precursor monocytes with rotenone inhibits the development of monocytes into immature DCs,<sup>80</sup> however, to our knowledge metformin’s DC-activating effects mediated via CI-i, shown here, have not been previously reported. If metformin inhibits the differentiation of monocytes to immature DC’s, but also simultaneously promotes DC activation, then what would be the net effect of metformin on the fully physiological TIME of BC? Since the evidence indicates that resident DCs within breast tissue are already in an immature DC state,<sup>81</sup> we propose that CI-i would immediately and beneficially target the tumor resident DCs by increasing tumor-antigen presentation by now-mature DCs. Therefore, adding metformin as an agent to explorative or standard cytotoxic treatments could leverage the tumor-antigen-releasing effects of the cytotoxic component, through simultaneously promoting DC-activation—a concept that should be especially considered in the scope of combination immunotherapies aimed at maintaining drug-induced T-cell responses.

Mechanistically, pharmacological inhibition of CI has a variety of different cell energy metabolism and oxidative stress-related effects, which alone or via additive or synergistic effects could explain the DC activation. While the exact mechanism of how CI-i induces DC maturation remains outside of the scope of the present study, we note that previous study has revealed an increase in DC

maturation and subsequent T-cell activation in response to free oxygen radicals,<sup>82</sup> which are in some circumstances released in response to respiratory CI-i. As an alternative to the causal role of free oxygen radicals, the DCs may undergo a “metabolic shift” in response to CI-i treatment.<sup>83–86</sup> DCs undergo a metabolic shift from oxidative phosphorylation to aerobic glycolysis in response to toll-like receptor agonists leading to DC maturation.<sup>52</sup> As metformin and CI-i decrease oxidative phosphorylation,<sup>87</sup> it is not inconceivable for a compensatory pathway to take over leading to DC maturation.

In summary, we demonstrate PDEC as a versatile preclinical immuno-oncology model of human TIME that can be easily adapted for a variety of research techniques like single-cell sequencing, and other studies that require the extraction of viable, single cells. Using the PDEC-TIME model, we reveal a hitherto unknown role of metformin for the maturation of APCs, specifically DCs, highlighting the potential clinical translatability of CI-i as means of boosting immunotherapy treatments.

## MATERIALS AND METHODS

### Cell lines and reagents

Human PBMCs were cultured in Roswell Park Memorial Institute (RPMI) medium supplemented with 10% heat-inactivated fetal bovine serum (FBS) (Biowest), 100 U penicillin–streptomycin (Gibco), and 2 mM L-Glutamine (Gibco). PDECs were cultured in MammoCult (STEMCELL Technologies), and the MammoCult media was supplemented with MammoCult proliferation supplement #05622 (STEMCELL Technologies), 20 µg/mL gentamicin (Sigma), 0.1 µg/mL amphotericin B (Biowest) and 10,000 U/mL penicillin/streptomycin (Lonza). Cells and PDECs were grown in a humidified incubator at 37°C under 5% CO<sub>2</sub>, and atmospheric oxygen levels.

PDECs were treated with 25 µl/mL anti-CD3/CD28/CD2 (STEMCELL Technologies), 100 µg/mL atezolizumab (Selleck Chemicals), 50 µg/mL pembrolizumab (MedChem), 10–100 nM Venetoclax (MedChem Express), 5–10 mM metformin (MedChem Express), 10–50 nM paclitaxel (MedChem Express), 1–2.5 nM IACS-010759 (Selleck Chemicals), 10–30 nM rotenone (Sigma-Aldrich), and 10 nM–1 µM A-769662 (Sigma-Aldrich), 100 ng/mL lipopolysaccharide (LPS).

### Isolation of biological material and three-dimensional culture

Fresh tissue was obtained from the elective BC surgeries performed at the Helsinki University Central Hospital (online supplemental figure 9A,B) (Ethical permit: 243/13/03/02/2013/TMK02 157 and HUS/2697/2019 approved by the Helsinki University Hospital Ethical Committee). Patients participated in the study by signing an informed consent form. Tissues were collected from tumors. From each tumor, a portion was taken for immunohistochemical, a second portion was frozen at –80°C DNA/RNA/protein analysis, and the remainder was used for the 3D cultures. Explants were produced by

incubating the samples overnight in collagenase A (3 mg/mL; Sigma) containing MammoCult media (STEMCELL Technologies) with gentle shaking (130 rpm) at +37°C. The resulting explants were collected via centrifugation at 353 rcf for 5 min and washed once with 1× phosphate-buffered saline (PBS). Isolated explants were embedded in Cultrex Reduced Growth Factor Basement Membrane Extract, Type 2 (R&D Systems) and plated on 8-Chamber Slides (Thermo Scientific).

### Flow cytometry

Explants were harvested by washing the wells twice with 1× PBS, then resuspended in 400 µL +4°C Cultrex Organoid Harvesting Solution (Bio-Techne Sales) and incubated at +4°C with gentle shaking for 30 min. Samples were pipetted onto Falcon round-bottom tubes with cell strainer caps (Corning) and centrifuged at 400 rcf for 5 min at +4°C. Samples were resuspended in 100 µL of flow cytometry staining buffer (1× PBS, 10% heat-inactivated FBS (Gibco)) and the appropriate antibodies (online supplemental table 1) for 45 min at +4°C in the dark. Samples were washed twice with flow cytometry running buffer (1× PBS, 1% heat-inactivated FBS (Gibco)), and resuspended in running buffer for analysis.

Samples were sorted with BD Influx or Sony SH800Z, or analyzed using BD FACSAria II, or NovoCyte Quanteon (Biomedicum Flow Cytometry Unit). Analysis was done using FlowJo V.10.8.1, and graphs were generated using GraphPad Prism V.9.

Flow cytometry antibodies are listed in online supplemental table 1.

### Macrophage polarization assay

CD14+ monocytes were isolated using positive magnetic separation with manufacturer instructions (Miltenyi) and were cultured in Iscove's modified Dulbecco's medium (Thermo Fisher) supplemented with 10% heat-inactivated FBS (Gibco), penicillin/streptomycin, and 50 ng/mL human M-CSF (Miltenyi Biotec). Monocytes were plated into 6-well plates ( $5 \times 10^5$  cells) and incubated for 6 days with one medium change. Media from differentiated macrophages was replaced with fresh media containing drugs. The adherent macrophages were detached using macrophage detachment solution DXF (Sigma-Aldrich) for 40 min at +4°C, washed with flow cytometry running buffer, and blocked with Fc-blocking antibody (eBioscience) in flow cytometry running buffer for 10 min at room temperature (according to manufacturer instructions) before adding fluorescent antibodies. Macrophage median fluorescence intensity of surface CD163 and CD206 expression was analyzed on the NovoCyte Quanteon flow cytometer.

### Dendritic cell activation assay

CD14+ monocytes were isolated using positive magnetic separation according to manufacturer protocol (Miltenyi Biotec) and cultured in RPMI medium supplemented with 10% heat-inactivated FBS (Biowest), 100 U

penicillin–streptomycin (Gibco), and 2 mM L-Glutamine (Gibco) with added 100 ng/mL Human granulocyte-macrophage colony-stimulating factor (GM-CSF) (Miltenyi Biotec), and 100 ng/mL Human IL-4 (Miltenyi Biotec) for 5 days only adding media once in between. On day 5, DCs were harvested and plated on a 96-well flat-bottom plate. Samples were incubated with 200 µL fresh media containing drugs for 48 hours. DCs were harvested and analyzed using flow cytometry on NovoCyte Quanteon. DCs expressing high levels of HLA-DR and CD86 were considered activated.

### T-cell proliferation assay

T cells were isolated using Pan T magnetic isolation beads (Miltenyi Biotec) according to manufacturer protocol, and stained with 1 µM carboxyfluorescein succinimidyl ester (CFSE) in 1× PBS in 37°C 5% CO<sub>2</sub> for 10 min before washing the samples with media. Stained T cells were co-cultured with autologous DCs at a ratio of 5:1 (T:DC) in DC media. 100 ng/mL of Ultra-Leaf purified anti-human CD3 (BioLegend 300413) was added to each sample, and anti-CD3/CD28/CD2, ImmunoCult (STEMCELL Tech) was used as a positive control. Samples were incubated for 72 hours at 37°C 5% CO<sub>2</sub> before being harvested and analyzed using flow cytometry. T-cell proliferation was quantified as the division index and proliferation index as calculated by FlowJo V.10.8.1 software.

Division index: Total number of divisions/the number of cells at the start of the culture.

Proliferation index: Total number of divisions/cells that went into division.

### scRNA sequencing and analysis

PDEC samples were harvested and stained with CD45+ to isolate CD45+ leukocytes with fluorescence-activated cell sorting from the total tumor tissue. Up to 30,000 CD45+ cells were collected for single cell 3' v3 library preparation with 10x Genomics Chromium. These single-cell libraries were sequenced on an Illumina NovaSeq 6000. Raw data were demultiplexed, aligned to GRCh38-2020-A and gene count data were generated by Cell Ranger (cellranger-4).

Raw count matrices were further analyzed in Seurat. Barcodes with <20% mtRNA, >400 unique read-counts, and a number of features between 200 and 6,000 were retained as cells.

Next, the data were integrated using Seurat's canonical-correlation-analysis,<sup>88</sup> clustered and visualized by uniform manifold approximation and projection (UMAP). Cell types were identified based on established marker genes. Significantly enriched cell types between cultured and tissue samples were calculated using the MASC algorithm.<sup>89</sup> The copy-number variation was assessed with inferCNV (<https://github.com/broadinstitute/inferCNV>) to identify the clusters of cancer cells. Preprocessed data may be found deposited online.<sup>90</sup>

### Seahorse extracellular flux assay

CD14<sup>+</sup> monocytes were isolated using positive magnetic separation according to manufacturer protocol (Miltneyi Biotec) and cultured in RPMI medium supplemented with 10% heat-inactivated FBS (Biowest), 100 U penicillin–streptomycin (Gibco), and 2 mM L-Glutamine (Gibco) with added 100 ng/mL Human GM-CSF (PeproTech), and 10 ng/mL Human IL-4 (PeproTech) for 5 days only adding media once in between. The immature DCs were then treated with either 5 mM or 10 mM metformin for 24 hours. The cells were collected and centrifuged (200 g, 5 min) and resuspended in Agilent RPMI assay medium containing 10 mM glucose (Agilent), 100 mM pyruvate (Agilent), and 200 mM glutamine (Agilent). 50  $\mu$ L of cell suspension was pipetted into the Agilent cell culture microplate (Agilent 103794–100) precoated with CellTak (Corning). Cells were centrifuged 200 g, 1 min with no brakes, and then incubated without CO<sub>2</sub> for 25 min as the drug-containing calibration cartridge was calibrating in the Seahorse XFe96. 130  $\mu$ L more of assay medium was pipetted per sample, and after another 20 min of incubation with 37°C, no CO<sub>2</sub>, the samples were analyzed for metabolic changes following the injection of 1.5  $\mu$ M oligomycin (TargetMol), 1  $\mu$ M FCCP (TargetMol), 0.5  $\mu$ M rotenone (Sigma-Aldrich)+0.5  $\mu$ M antimycin (Sigma-Aldrich), and 1:5,000 dilution of Hoechst (Thermo Scientific) using the standard reading frame per injection of 3 min mix, 0 min wait, 3 min measure. The number of technical repeats was based on available cell numbers.

### 3' RNA sequencing

Total RNA was isolated using RNeasy Plus (Qiagen) which contains a genomic deoxyribonucleic acid (gDNA) eliminator column. RNA sequencing libraries were prepared from 100 ng of total RNA using either the ScriptSeq Complete Gold Kit or the NEBNext Ultra Directional RNA Library Prep Kit for Illumina depending on the RNA integrity. Using the ScriptSeq Complete Gold Kit, the ribosomal RNA was removed first from the total RNA using the Ribo-Zero Gold rRNA Removal Kit after which the RNA was fragmented chemically. The libraries were prepared according to the manufacturer's instructions. Finally, the library was assessed with the Agilent Bioanalyzer.

The NEBNext Ultra Directional RNA Library Prep Kit for Illumina was used to generate the complementary DNA (cDNA) libraries for next-generation sequencing. First, the ribosomal RNA-depleted samples (10 ng) were fragmented to generate the inserts around 200 bp. The libraries were prepared according to the manufacturer's instructions. The library quality was assessed with Bioanalyzer (Agilent DNA High Sensitivity chip) and the library quantity with the Qubit (Invitrogen).

Samples were sequenced with the NextSeq 500—Illumina instrument using 75 Paired-End reads with a sequencing depth of 33 M reads/sample. Differentially expressed genes between different groups were found using state-of-the-art statistical methods and packages,

such as edgeR/DESeq2. The Gene Set Enrichment Analysis (GSEA) V.3.0 (Broad Institute) was used to analyze the differences in the gene expression profiles. GSEA results were visualized using GraphPad Prism V.9.5.0. Data can be found deposited online.<sup>90</sup>

### Mouse tissue spatial transcriptomics

Two cryopreserved tumor tissue sections from one metformin-treated and one untreated Wap-Myc mice were profiled for spatial transcriptomics using the 10x Genomics Visium spatial RNA-sequencing technology with a resolution of 55  $\mu$ m per spot. The tissues were cryosectioned at 10  $\mu$ m thickness onto the Visium library preparation slide, fixed in methanol for 30 min, stained with Hematoxylin and Eosin Stain Kit (Vector Laboratories) and stored at –20°C until library preparation. The slide was imaged using Zeiss Axio Imager.

Sequencing library preparation was performed according to the Visium Spatial Gene Expression user guide (CG000239 RevC, 10x Genomics) using a 12 min tissue-permeabilization time that was tested earlier with the Tissue Optimization Slide to be optimal for the mouse tumor tissues.

Libraries were sequenced with Illumina NovaSeq 6000 sequencer at the FIMM Genomics core facility at the University of Helsinki, with the aimed depth of 75 million reads per section (corresponding to approximately 50,000 reads per tissue-covered array spot).

The analysis was done using R V.4.2.2 and Seurat V.4.3.0. In order to maintain only good quality spots and relevant spots in analysis, spots with lesser than 500 Features or more than 25% of mitochondrial transcripts or more than 1% of hb transcripts were excluded from the analysis. Data was normalized using SCTransform<sup>91</sup> and afterward, principal component analysis and dimension reduction with UMAP<sup>92</sup> was done with default parameters and with Seurat functions accordingly. Identification of clusters was done with Seurat FindClusters function and a resolution of 0.8. Top significantly (p value adjusted <0.05) differentially expressed genes (online supplemental figure 5C,D) obtained from Seurat FindMarkers function (Wilcoxon rank-sum test) were used for cluster annotation. Differentially expressed genes between different tumor areas were defined by using the same function and Wilcoxon rank-sum test.

### NanoString gene expression profiling

Total RNA was isolated using RNeasy (Qiagen), and the DNAase removal step was performed after the isolation (Zymo research). Samples went through QC (Qubit), gene expression analysis was conducted on the NanoString nCounter gene expression platform (NanoString Technologies). Due to the systemic reduction of TILs in explants, the samples were normalized to the genes that create the TIL score: T cell, CD45, B cell, cytotoxic cell, and macrophage genes excluding those with counts below 100 (*CD3G*, *CD3D*, *CD3E*, *SH2D1A*, *CD6*, *PTPRC*, *BLK*, *MS4A1*, *TNGFRSF17*, *CD19*, *CD84*, *CD68*, *CD163*, *CTSW*,

*KLRB1, KLRD1, GzMB, PRF1, GZMA, GNLY, KLRK1, GZMH, CD8, CD8A, CD8B, CD4*) before comparing activity profiles. Significance was calculated with nSolver's directional significance score calculated as t-statistic for each gene against each covariate in the model, taking the sign of the t-statistics into account.

nCounter Human PanCancer Immune Profiling Panel consisting of 770 genes from different immune cell types, common checkpoint inhibitors, CT antigens, and genes covering both the adaptive and innate immune response. Per sample, 50 ng of total RNA in a final volume of 5  $\mu$ L was mixed with a reporter codeset, and hybridization buffer, and capture codeset. Samples were hybridized overnight at 65°C for 20 hours. Hybridized samples were run on the NanoString nCounter SPRINT profiler. Data set found deposited online.<sup>90</sup>

### Multiplex and standard immunohistochemistry

Tissues and explant cultures were fixed with 4% paraformaldehyde (PFA) and embedded in paraffin. The samples were sectioned into 5  $\mu$ m slices and deparaffinized. The heat-induced antigen retrieval was performed with a microwave oven or a pressure cooker in a citrate buffer solution (Dako). Histochemical stainings were carried out using standard techniques for IHC and IHC-IF. Images were taken with a Leica DM LB microscope or with a Zeiss AxioImager 1 (Biomedicum Imaging Unit, University of Helsinki). Multiplex images were stained in two rounds and tissue sections were scanned on the Zeiss AxioImager Z1 scanner at FL20X.

The list of used antibodies is shown in online supplemental table 2.

### Immunofluorescent staining

3D cultured BC explants were fixed with 4% PFA for 15 min at room temperature and washed three times with PBS. The tissue explants were permeabilized with 0.5% Triton X-100 in PBS for 10 min at room temperature (RT) and blocked in an IF buffer (0.1% BSA, 0.2% Triton X-100, 7.7 mM NaN<sub>3</sub>, and 0.05% Tween 20 in PBS) supplemented with 10% (v/v) normal goat serum for 1 hour. Explants were then incubated with the primary antibody diluted in a blocking solution overnight at 4°C. Following incubation, explants were washed three times with an IF buffer and then incubated using the appropriate Alexa Fluor secondary antibody diluted in an IF buffer with 10% goat serum. After 60 min of incubation at RT, the explants were washed with an IF buffer as before and the nuclei were counterstained with Hoechst 33258 (Sigma). Instead of antibodies, cell death staining was done with the CellTox green (Promega) at a dilution of 0.25  $\mu$ L CellTox/500  $\mu$ L media for 20 min. Samples were then washed twice with 1 $\times$  PBS, fixed with 2% PFA for 20 min, washed twice with 1 $\times$  PBS, and stored in +4°C until imaging. Slides containing tissue explants were mounted with the ImmuMount reagent (Fisher Scientific). Images of the structures were acquired using a Leica TCS SP8 CARS confocal microscope using an HC PL APO CS2

40 $\times$  objective (Biomedicum Imaging Unit, University of Helsinki).

### Cytokine profiling

PDEC cytokine secretion was analyzed from cleared PDEC culture supernatants using Bio-Plex Pro Human Cytokine 27-plex assay kit (Bio-Rad, cat. M500KCAF0Y) and Bio-Plex 200 System (Bio-Rad) according to the manufacturer's instructions. Results were analyzed using Bio-Plex Manager V.6.0 software (Bio-Rad Laboratories).

Cytokines with >10% of data points outside the detection range were excluded from the analyses. Remaining values lower than the detection limit were replaced by 0.5' lowest measured value. Further data analyses and visualizations were performed using R (V.4.0.4,<sup>93</sup> tidyverse V.1.3.1). To identify changes in untreated PDEC cytokine secretion over time, we calculated  $\log_2$ foldchanges between day 6 and day 3 cytokine levels and analyzed their deviance from 0 (unchanged) with one-sample t-test. The resulting Benjamini-Hochberg-adjusted p values and average  $\log_2$ foldchanges were visualized as a volcano plot. For comparing different treatments, we used dimethyl sulfoxide (DMSO)-treated PDEC cytokine levels as a baseline and calculated  $\log_2$ foldchanges for the indicated treatments. Unsupervised hierarchical clustering was performed with R (function hclust) based on  $\log_2$ foldchanges and visualized as a heatmap using ComplexHeatmap package (V.2.6.2).<sup>94</sup> Bar graphs (median $\pm$ IQR) and line plots (median) were plotted using  $\log_2$ foldchange values, and statistical significances were reported as Benjamini-Hochberg adjusted p values from one-sample Wilcoxon signed-rank tests (deviance from zero).

### q-PCR analysis

Total RNA was isolated from cell lines and primary cell cultures using the Qiagen RNEasy Kit according to the manufacturer's instructions, while the cDNA synthesis was performed with the Maxima First Strand cDNA Synthesis Kit for real-time quantitative polymerase chain reaction (RT-qPCR) (Thermo Scientific). RT-qPCR was performed with LightCycler 480 II (Roche) using DyNAmo Color-Flash SYBR Green (Thermo Scientific). The gene-specific primer sets were used at a final concentration of 0.2 mM.

Primers are listed in online supplemental table 3.

### Statistical analysis

We report our results as the mean $\pm$ SD. Data sets were analyzed using Fisher's exact test. All the experiments with representative images (immunohistology, and immunofluorescence stainings) have been repeated at least thrice. When comparing multiple groups, the p values were calculated using one-way analysis of variance, unless otherwise specified in the figure legend.

### Author affiliations

<sup>1</sup>Translational Cancer Medicine, University of Helsinki, Helsinki, Finland

<sup>2</sup>University of Turku, Turku, Finland



<sup>3</sup>KU Leuven, Leuven, Belgium

<sup>4</sup>Department of Human Genetics, KU Leuven, Leuven, Belgium

<sup>5</sup>University of Helsinki Faculty of Medicine, Helsinki, Finland

<sup>6</sup>Scellex, Helsinki, Finland

<sup>7</sup>Department of Pathology, Helsinki University Central Hospital, Helsinki, Finland

<sup>8</sup>Department of Pathology, HUSLAB, Helsinki University Central Hospital, Helsinki, Finland

<sup>9</sup>Breast Surgery Unit, Helsinki University Central Hospital Comprehensive Cancer Center, Helsinki, Finland

<sup>10</sup>Department of oncology, Helsinki University Central Hospital, Helsinki, Finland

<sup>11</sup>TRIMM, Translational Immunology Research Program, University of Helsinki, Helsinki, Finland

<sup>12</sup>University of Helsinki Helsinki Institute of Life Sciences, Helsinki, Finland

<sup>13</sup>Department of Cell & Tissue Biology, UCSF, San Francisco, California, USA

<sup>14</sup>VIB–KU Leuven Center for Cancer Biology, Leuven, Belgium

<sup>15</sup>Finnish Cancer Institute, Helsinki, Finland

X Rita Turpin @CancerResearch, Satu Mustjoki @hruh\_research and Juha Klefström @KlefstromLab

**Acknowledgements** We are grateful to the patients who participated in this research by donating breast tumor tissue samples and made it possible, and to the surgical personnel at Helsinki University Hospital who assisted with the recruitment and collection of the sample material. We are grateful to Biomedicum Imaging Unit (BIU), Biomedicum Functional Genomics Unit (FuGU), and Biomedicum Flow Cytometry Unit (from HiLIFE, University of Helsinki and Biocenter Finland) for their services. We thank the Klefström laboratory personnel for discussions and critical comments on the manuscript. Schematic images were created with BioRender.com. We thank the Finnish Cancer Institute (FCI) for financial support.

**Contributors** RT and JK wrote the paper, conceived and designed the analysis. MH, JP, DL, AG, PS, SM and MM conceived and designed the analysis, data analysis and interpretation. RT, RL, PMM, AP, JHR, GP, BB, NS, EH, IS, JA, EMV, LL and MM collected the data, contributed data and analysis tools. JM, TM, LN and PK collected the data. JK is the guarantor of this study.

**Funding** This work was supported by grants from the Academy of Finland, Business Finland, the Finnish Cancer Organizations, Sigrid Juséliuksen Säätiö, Jane and Aatos Erkon Säätiö, the Research Council of Finland, and RESCUER project, which has received funding from the European Union's Horizon 2020 Framework Programme (no. 847912). This work was also supported by the US Department of Defense for Health Affairs through the Breast Cancer Research Program under (award no. W81XWH2110773). Opinions, interpretations, conclusions, and recommendations are those of the author and are not necessarily endorsed by the Department of Defense. In addition, funds were received from Sihtasutus Archimedes, Ida Montinin Säätiö, Finnish Cancer Institute, Syöpäjärjestöt, and the iCAN Digital Precision Cancer Medicine Flagship.

**Competing interests** MH is an employee, owns shares and has received research funding from Faron Pharmaceuticals.

**Patient consent for publication** Not applicable.

**Ethics approval** Fresh tissue was obtained from the elective breast cancer surgeries performed at the Helsinki University Central Hospital (Ethical permit: 243/13/03/02/2013/ TMK02 157 and HUS/2697/2019 approved by the Helsinki University Hospital Ethical Committee). Participants gave informed consent to participate in the study before taking part.

**Provenance and peer review** Not commissioned; externally peer reviewed.

**Data availability statement** Data are available upon reasonable request. Source data for BRB sequencing, scSequencing, and gene expression profiling can be found deposited at <https://doi.org/10.5281/zenodo.7906989> under the Creative Commons Attribution 4.0 International license. All other manuscript data are available from the authors upon reasonable request. All data relevant to the study are included in the article or uploaded as supplementary information.

**Supplemental material** This content has been supplied by the author(s). It has not been vetted by BMJ Publishing Group Limited (BMJ) and may not have been peer-reviewed. Any opinions or recommendations discussed are solely those of the author(s) and are not endorsed by BMJ. BMJ disclaims all liability and responsibility arising from any reliance placed on the content. Where the content includes any translated material, BMJ does not warrant the accuracy and reliability of the translations (including but not limited to local regulations, clinical guidelines,

terminology, drug names and drug dosages), and is not responsible for any error and/or omissions arising from translation and adaptation or otherwise.

**Open access** This is an open access article distributed in accordance with the Creative Commons Attribution Non Commercial (CC BY-NC 4.0) license, which permits others to distribute, remix, adapt, build upon this work non-commercially, and license their derivative works on different terms, provided the original work is properly cited, appropriate credit is given, any changes made indicated, and the use is non-commercial. See <http://creativecommons.org/licenses/by-nc/4.0/>.

#### ORCID iDs

Satu Mustjoki <http://orcid.org/0000-0002-0816-8241>

Juha Klefström <http://orcid.org/0000-0001-7124-8431>

#### REFERENCES

- Chen DS, Mellman I. Elements of cancer immunity and the cancer-immune set point. *Nature* 2017;541:321–30.
- Ye Y, Zhang Y, Yang N, *et al.* Profiling of immune features to predict immunotherapy efficacy. *Innovation (Camb)* 2022;3:100194.
- Chen DS, Mellman I. Oncology meets immunology: the cancer-immunity cycle. *Immunity* 2013;39:1–10.
- Sharma P, Allison JP. Immune checkpoint targeting in cancer therapy: toward combination strategies with curative potential. *Cell* 2015;161:205–14.
- Mackall CL, Fleisher TA, Brown MR, *et al.* Lymphocyte depletion during treatment with intensive chemotherapy for cancer. *Blood* 1994;84:2221–8.
- Verma R, Foster RE, Horgan K, *et al.* Lymphocyte depletion and repopulation after chemotherapy for primary breast cancer. *Breast Cancer Res* 2016;18:10.
- Ruffell B, Coussens LM. Macrophages and therapeutic resistance in cancer. *Cancer Cell* 2015;27:462–72.
- Shree T, Olson OC, Elie BT, *et al.* Macrophages and cathepsin proteases blunt chemotherapeutic response in breast cancer. *Genes Dev* 2011;25:2465–79.
- Rugo HS, Delord J-P, Im S-A, *et al.* Safety and antitumor activity of Pembrolizumab in patients with estrogen receptor–positive/human epidermal growth factor receptor 2–negative advanced breast cancer. *Clin Cancer Res* 2018;24:2804–11.
- Dirix LY, Takacs I, Jerusalem G, *et al.* Avelumab, an anti-PD-L1 antibody, in patients with locally advanced or metastatic breast cancer: a phase 1B JAVELIN solid tumor study. *Breast Cancer Res Treat* 2018;167:671–86.
- Adams S, Loi S, Toppmeyer D, *et al.* Pembrolizumab monotherapy for previously untreated, PD-L1–positive, metastatic triple-negative breast cancer: cohort B of the phase II KEYNOTE-086 study. *Ann Oncol* 2019;30:405–11.
- Ademuyiwa FO, Gao F, Chen I, *et al.* Abstract PD14-09: NCI 10013 – A randomized phase 2 study of neoadjuvant carboplatin and paclitaxel, with or without Atezolizumab in triple negative breast cancer (TNBC). *Cancer Res* 2021;81:PD14-09.
- Schmid P, Rugo HS, Adams S, *et al.* Atezolizumab plus NAB-paclitaxel as first-line treatment for Unresectable, locally advanced or metastatic triple-negative breast cancer (Impassion130): updated efficacy results from a randomised, double-blind, placebo-controlled, phase 3 trial. *Lancet Oncol* 2020;21:44–59.
- Upadhaya S, Neftelino ST, Hodge JP, *et al.* Combinations take centre stage in PD1/PDL1 inhibitor clinical trials. *Nat Rev Drug Discov* 2021;20:168–9.
- Lv B, Wang Y, Ma D, *et al.* Immunotherapy: reshape the tumor immune microenvironment. *Front Immunol* 2022;13:844142.
- De Henau O, Rausch M, Winkler D, *et al.* Overcoming resistance to checkpoint blockade therapy by targeting PI3Kγ in myeloid cells. *Nature* 2016;539:443–7.
- O'Neil NJ, Bailey ML, Hieter P. Synthetic lethality and cancer. *Nat Rev Genet* 2017;18:613–23.
- Dang CV. MYC on the path to cancer. *Cell* 2012;149:22–35.
- Nieminen AI, Partanen JI, Hau A, *et al.* c-Myc primed mitochondria determine cellular sensitivity to TRAIL-induced apoptosis. *EMBO J* 2007;26:1055–67.
- Pelengaris S, Khan M, Evan G. c-Myc: more than just a matter of life and death. *Nat Rev Cancer* 2002;2:764–76.
- Juin P, Hunt A, Littlewood T, *et al.* C-Myc functionally cooperates with BAX to induce apoptosis. *Mol Cell Biol* 2002;22:6158–69.
- Klefstrom J, Arighi E, Littlewood T, *et al.* Induction of TNF-sensitive cellular phenotype by c-Myc involves P53 and impaired NF-KB activation. *EMBO J* 1997;16:7382–92.

- 23 Thng DKH, Toh TB, Chow EKH. Capitalizing on synthetic lethality of MYC to treat cancer in the digital age. *Trends Pharmacol Sci* 2021;42:166–82.
- 24 Donati G, Amati B. MYC and therapy resistance in cancer: risks and opportunities. *Mol Oncol* 2022;16:3828–54.
- 25 Horiuchi D, Anderton B, Goga A. Taking on challenging targets: making Myc druggable. *Am Soc Clin Oncol Educ Book* 2014:e497–502.
- 26 Souers AJ, Levenson JD, Boghaert ER, et al. ABT-199, a potent and selective BCL-2 inhibitor, achieves antitumor activity while sparing platelets. *Nat Med* 2013;19:202–8.
- 27 Haikala HM, Anttila JM, Marques E, et al. Pharmacological reactivation of MYC-dependent apoptosis induces susceptibility to anti-PD-1 Immunotherapy. *Nat Commun* 2019;10:620.
- 28 Eikawa S, Nishida M, Mizukami S, et al. Immune-mediated antitumor effect by type 2 diabetes drug, metformin. *Proc Natl Acad Sci U S A* 2015;112:1809–14.
- 29 Cha J-H, Yang W-H, Xia W, et al. Metformin promotes antitumor immunity via Endoplasmic-Reticulum-associated degradation of PD-L1. *Mol Cell* 2018;71:606–20.
- 30 Zhang Z, Li F, Tian Y, et al. Metformin enhances the antitumor activity of CD8+ T lymphocytes via the AMPK–miR-107–Eomes–PD-1 pathway. *J Immunol* 2020;204:2575–88.
- 31 Al-Akhrass H, Pietilä M, Lilja J, et al. Sortilin-related receptor is a druggable therapeutic target in breast cancer. *Mol Oncol* 2022;16:116–29.
- 32 Munne PM, Martikainen L, Rätty I, et al. Compressive stress-mediated P38 activation required for ER $\alpha$  + phenotype in breast cancer. *Nat Commun* 2021;12:6967.
- 33 Tervonen TA, Belitškin D, Pant SM, et al. Deregulated Hepsin protease activity confers Oncogenicity by concomitantly augmenting HGF/MET signalling and disrupting epithelial cohesion. *Oncogene* 2016;35:1832–46.
- 34 Kohlhapp FJ, Haribhai D, Mathew R, et al. Venetoclax increases intratumoral effector T cells and antitumor efficacy in combination with immune checkpoint blockade. *Cancer Discov* 2021;11:68–79.
- 35 Voabil P, de Bruijn M, Roelofs LM, et al. An ex vivo tumor fragment platform to dissect response to PD-1 blockade in cancer. *Nat Med* 2021;27:1250–61.
- 36 Voskoboinik I, Dunstone MA, Baran K, et al. Perforin: structure, function, and role in human immunopathology. *Immunol Rev* 2010;235:35–54.
- 37 Shankaran V, Ikeda H, Bruce AT, et al. IFN $\gamma$  and lymphocytes prevent primary tumour development and shape tumour immunogenicity. *Nature* 2001;410:1107–11.
- 38 Sabat R, Grütz G, Warszawska K, et al. Biology of Interleukin-10. *Cytokine Growth Factor Rev* 2010;21:331–44.
- 39 Malek TR. The biology of Interleukin-2. *Annu Rev Immunol* 2008;26:453–79.
- 40 Urbaniak A, Piña-Oviedo S, Yuan Y, et al. Limitations of an ex vivo breast cancer model for studying the mechanism of action of the anticancer drug paclitaxel. *Eur J Pharmacol* 2021;891:173780.
- 41 Gerhard GM, Bill R, Messemaker M, et al. Tumor-infiltrating Dendritic cell states are conserved across solid human cancers. *J Exp Med* 2021;218:e20200264.
- 42 Michea P, Noël F, Zakine E, et al. Adjustment of Dendritic cells to the breast-cancer microenvironment is subset specific. *Nat Immunol* 2018;19:885–97.
- 43 Uehara T, Eikawa S, Nishida M, et al. Metformin induces CD11B+ Cell-mediated growth inhibition of an osteosarcoma: implications for metabolic reprogramming of myeloid cells and anti-tumor effects. *Int Immunol* 2019;31:187–98.
- 44 Chiang C-F, Chao T-T, Su Y-F, et al. Metformin-treated cancer cells modulate macrophage polarization through AMPK-NF-KB signaling. *Oncotarget* 2017;8:20706–18.
- 45 Ding L, Liang G, Yao Z, et al. Metformin prevents cancer metastasis by inhibiting M2-like polarization of tumor associated macrophages. *Oncotarget* 2015;6:36441–55.
- 46 Wang J-C, Sun X, Ma Q, et al. Metformin's antitumor and anti-angiogenic activities are mediated by skewing macrophage polarization. *J Cell Mol Med* 2018;22:3825–36.
- 47 Bridges HR, Blaza JN, Yin Z, et al. Structural basis of mammalian respiratory complex I inhibition by medicinal Biguanides. *Science* 2023;379:351–7.
- 48 Zhou G, Myers R, Li Y, et al. Role of AMP-activated protein kinase in mechanism of metformin action. *J Clin Invest* 2001;108:1167–74.
- 49 Vancura A, Bu P, Bhagwat M, et al. Metformin as an anticancer agent. *Trends Pharmacol Sci* 2018;39:867–78.
- 50 Tsuji A, Akao T, Masuya T, et al. IACS-010759, a potent inhibitor of glycolysis-deficient hypoxic tumor cells, inhibits mitochondrial respiratory complex I through a unique mechanism. *J Biol Chem* 2020;295:7481–91.
- 51 Nurieva R, Thomas S, Nguyen T, et al. T-cell tolerance or function is determined by combinatorial costimulatory signals. *EMBO J* 2006;25:2623–33.
- 52 Krawczyk CM, Holowka T, Sun J, et al. Toll-like receptor-induced changes in glycolytic metabolism regulate Dendritic cell activation. *Blood* 2010;115:4742–9.
- 53 Upadhaya S, Neftelinov ST, Hodge J, et al. Challenges and opportunities in the PD1/PDL1 inhibitor clinical trial landscape. *Nat Rev Drug Discov* 2022;21:482–3.
- 54 Palucka AK, Coussens LM. The basis of Oncoimmunology. *Cell* 2016;164:1233–47.
- 55 Klemm F, Joyce JA. Microenvironmental regulation of therapeutic response in cancer. *Trends Cell Biol* 2015;25:198–213.
- 56 Junttila MR, de Sauvage FJ. Influence of tumour micro-environment heterogeneity on therapeutic response. *Nature* 2013;501:346–54.
- 57 Bhatia S, Kramer M, Russo S, et al. Patient-derived triple-negative breast cancer Organoids provide robust model systems that recapitulate tumor intrinsic characteristics. *Cancer Res* 2022;82:1174–92.
- 58 Sachs N, de Ligt J, Kopper O, et al. A living Biobank of breast cancer organoids captures disease heterogeneity. *Cell* 2018;172:373–86.
- 59 Dekkers JF, van Vliet EJ, Sachs N, et al. Long-term culture, genetic manipulation and Xenotransplantation of human normal and breast cancer Organoids. *Nat Protoc* 2021;16:1936–65.
- 60 Zhou Z, Van der Jeught K, Fang Y, et al. An Organoid-based screen for epigenetic inhibitors that stimulate antigen presentation and potentiate T-cell-mediated cytotoxicity. *Nat Biomed Eng* 2021;5:1320–35.
- 61 Van den Eynde M, Mlecnik B, Bindea G, et al. The link between the multiverse of immune microenvironments in metastases and the survival of colorectal cancer patients. *Cancer Cell* 2018;34:1012–26.
- 62 Hirata E, Sahai E. Tumor microenvironment and differential responses to therapy. *Cold Spring Harb Perspect Med* 2017;7:a026781.
- 63 Hwang M, Canzoniero JV, Rosner S, et al. Peripheral blood immune cell dynamics reflect antitumor immune responses and predict clinical response to immunotherapy. *J Immunother Cancer* 2022;10:e004688.
- 64 Anderson KG, Stromnes IM, Greenberg PD. Obstacles posed by the tumor microenvironment to T cell activity: a case for synergistic therapies. *Cancer Cell* 2017;31:311–25.
- 65 Hegde PS, Karanikas V, Evers S. The where, the when, and the how of immune monitoring for cancer immunotherapies in the era of checkpoint inhibition. *Clin Cancer Res* 2016;22:1865–74.
- 66 Herbst RS, Soria J-C, Kowanetz M, et al. Predictive correlates of response to the anti-PD-L1 antibody MPDL3280A in cancer patients. *Nature* 2014;515:563–7.
- 67 Sharma P, Allison JP. The future of immune checkpoint therapy. *Science* 2015;348:56–61.
- 68 Galon J, Bruni D. Approaches to treat immune hot, altered and cold tumours with combination immunotherapies. *Nat Rev Drug Discov* 2019;18:197–218.
- 69 Yuki K, Cheng N, Nakano M, et al. Organoid models of tumor immunology. *Trends Immunol* 2020;41:652–64.
- 70 Jenkins RW, Aref AR, Lizotte PH, et al. Ex vivo profiling of PD-1 blockade using organotypic tumor spheroids. *Cancer Discov* 2018;8:196–215.
- 71 Lu P, Fleischmann R, Curtis C, et al. Safety and pharmacodynamics of Venetoclax (ABT-199) in a randomized single and multiple ascending dose study in women with systemic lupus erythematosus. *Lupus* 2018;27:290–302.
- 72 Kim IS, Gao Y, Welte T, et al. Immuno-subtyping of breast cancer reveals distinct myeloid cell profiles and immunotherapy resistance mechanisms. *Nat Cell Biol* 2019;21:1113–26.
- 73 Barry KC, Hsu J, Broz ML, et al. A natural killer–Dendritic cell axis defines checkpoint therapy–responsive tumor microenvironments. *Nat Med* 2018;24:1178–91.
- 74 Gabrilovich DI, Ostrand-Rosenberg S, Bronte V. Coordinated regulation of myeloid cells by tumours. *Nat Rev Immunol* 2012;12:253–68.
- 75 Honkanen TJ, Tikkanen A, Karihtala P, et al. Prognostic and predictive role of tumour-associated macrophages in Her2 positive breast cancer. *Sci Rep* 2019;9:10961.
- 76 Wei Z, Zhang X, Yong T, et al. Boosting anti-PD-1 therapy with metformin-loaded macrophage-derived microparticles. *Nat Commun* 2021;12:440.
- 77 Giles ED, Jindal S, Wellberg EA, et al. Metformin inhibits stromal aromatase expression and tumor progression in a rodent model of postmenopausal breast cancer. *Breast Cancer Res* 2018;20:50.
- 78 Hillenbrand EE, Neville AM, Coventry BJ. Immunohistochemical localization of CD1A-positive putative Dendritic cells in human breast tumours. *Br J Cancer* 1999;79:940–4.



- 79 La Rocca G, Anzalone R, Corrao S, *et al.* CD1A down-regulation in primary invasive Ductal breast carcinoma may predict regional lymph node invasion and patient outcome. *Histopathology* 2008;52:203–12.
- 80 Fato R, Bergamini C, Bortolus M, *et al.* Differential effects of mitochondrial complex I inhibitors on production of reactive oxygen species. *Biochimica et Biophysica Acta (BBA) - Bioenergetics* 2009;1787:384–92.
- 81 Bell D, Chomarat P, Broyles D, *et al.* In breast carcinoma tissue, immature Dendritic cells reside within the tumor, whereas mature Dendritic cells are located in peritumoral areas. *J Exp Med* 1999;190:1417–26.
- 82 Rutault K, Alderman C, Chain BM, *et al.* Reactive oxygen species activate human peripheral blood Dendritic cells. *Free Radic Biol Med* 1999;26:232–8.
- 83 Santos PM, Menk AV, Shi J, *et al.* Tumor-derived A-Fetoprotein suppresses fatty acid metabolism and oxidative phosphorylation in Dendritic cells. *Cancer Immunol Res* 2019;7:1001–12.
- 84 O'Neill LAJ, Pearce EJ. Immunometabolism governs Dendritic cell and macrophage function. *J Exp Med* 2016;213:15–23.
- 85 Liu P-S, Chen Y-T, Li X, *et al.* CD40 signal rewires fatty acid and Glutamine metabolism for stimulating macrophage anti-tumorigenic functions. *Nat Immunol* 2023;24:452–62.
- 86 Du X, Chapman NM, Chi H. Emerging roles of cellular metabolism in regulating Dendritic cell subsets and function. *Front Cell Dev Biol* 2018;6:152.
- 87 Foretz M, Guigas B, Bertrand L, *et al.* Metformin: from mechanisms of action to therapies. *Cell Metab* 2014;20:953–66.
- 88 Diemer J, Kelly M, Kwon EM, *et al.* Single cell RNA-sequencing to uncover cell type-specific gene expression changes during Inv(16) leukemia initiation. *Blood* 2018;132:1326.
- 89 Fonseka CY, Rao DA, Teslovich NC, *et al.* Mixed-effects association of single cells identifies an expanded effector CD4+ T cell subset in rheumatoid arthritis. *Sci Transl Med* 2018;10:eaq0305.
- 90 Turpin R, Liu R, Munne PM, *et al.* Respiratory complex I regulates Dendritic cell maturation in explant model of human tumor immune microenvironment. *bioRxiv* [Preprint] 2023.
- 91 Hafemeister C, Satija R. Normalization and variance stabilization of single-cell RNA-Seq data using regularized negative binomial regression. *Genome Biol* 2019;20:296.
- 92 Bro R, Smilde AK. Principal component analysis. *Anal Methods* 2014;6:2812–31.
- 93 R Core Team. R: A language and environment for statistical computing. *R Foundation for Statistical Computing* [Preprint] 2021.
- 94 Gu Z, Eils R, Schlesner M. Complex heatmaps reveal patterns and correlations in multidimensional genomic data. *Bioinformatics* 2016;32:2847–9.